Geological Magazine

www.cambridge.org/geo

Original Article

Cite this article: Liao W, Han B-F, Xu Y, and Li A (2021) Ediacaran initial subduction and Cambrian slab rollback of the Junggar Ocean: New evidence from igneous tectonic blocks and gabbro enclave in Early Palaeozoic accretionary complexes, southern West Junggar, NW China. *Geological Magazine* **158**: 1811–1829. https://doi.org/10.1017/S0016756821000376

Received: 20 November 2020
Revised: 17 March 2021
Accepted: 6 April 2021
First published online: 11 May 2021

Keywords:
initial subduction; Junggar Ocean; Ediacaran; adakite; slab rollback

Author for correspondence: Bao-Fu Han,
Email: bfhan@pku.edu.cn

Ediacaran initial subduction and Cambrian slab rollback of the Junggar Ocean: New evidence from igneous tectonic blocks and gabbro enclave in Early Palaeozoic accretionary complexes, southern West Junggar, NW China

Wen Liao, Bao-Fu Han, Yan Xu and Ang Li

Ministry of Education, Key Laboratory of Orogenic Belts and Crustal Evolution, School of Earth and Space Science, Peking University, Beijing 100871, China

Abstract

New zircon U–Pb ages and whole-rock chemical data from four adakitic and two non-adakitic igneous rocks as tectonic blocks in the southern West Junggar accretionary complexes, northwestern China and one gabbro enclave in adakitic block provide further constraints on the initial subduction and following rollback process of the Junggar Ocean as part of southern Palaeo-Asian Ocean. The oldest adakitic monzonite in Tangbale is intruded by the non-adakitic quartz monzonite at 549 Ma, and the youngest adakitic diorite in Tierekehuola formed at 520 Ma. The Ediacaran–Cambrian magmatism show a N-wards younger trend. The high-SiO_2 adakitic rocks have high Sr (300–663 ppm) and low Y (6.68–12.2 ppm), with Sr/Y = 40–84 and Mg no. = 46–60, whereas the non-adakitic rocks have high Y (13.2–22.7 ppm) and Yb (2.32–2.92 ppm), with Mg no. = 36–40. The gabbro has high MgO (14.81–15.11 wt%), Co (45–48 ppm), Cr (1120–1360 ppm) and Ni (231–288 ppm), with Mg no. = 72–73. All the samples show similar large-ion lithophile element (LILE) and light rare earth element (LREE) enrichment and Nb, Ta, Ti and varying Zr and Hf depletion, suggesting that they were formed in a subduction-related setting. The adakitic rocks were produced by partial melting of subducted oceanic slab, but the melts were modified by mantle wedge and slab-derived fluids; the non-adakitic rocks were likely derived from partial melts of the middle-lower arc crust; and the gabbro originated from the mantle wedge modified by slab-derived fluids. The magmatism could have been generated during the Ediacaran initial subduction and Cambrian slab rollback of the Junggar Ocean.

1. Introduction

Initial subduction refers to the first sinking of oceanic lithosphere into the mantle, when the subduction zone still has the thermal structure of an unstable state (Agard *et al.* 2016). With respect to the initial subduction of an ancient ocean, the oldest supra-subduction zone (SSZ-type) ophiolite, island-arc igneous rocks and subduction-related metamorphic rocks in accretionary complexes can provide important constraints on the timing of initial subduction (Guilmette *et al.* 2018; Stern & Taras, 2018).

The Central Asian Orogenic Belt (CAOB) between the Siberian Craton and the Tarim–North China Craton is one of the largest accretionary orogenic belts on Earth, and its formation was closely related to the evolution of Neoproterozoic–Palaeozoic Palaeo-Asian Ocean (PAO) (Fig. 1a; Xiao *et al.* 2003, 2015; Kröner *et al.* 2007; Windley *et al.* 2007). The subduction of the northern PAO was initiated prior to *c.* 1000 Ma, SSZ-type ophiolites at 1020–1017 Ma (Khain *et al.* 2002; Turkina *et al.* 2004) and arc-complex at 972–826 Ma (Nekrasov *et al.* 2007; Gordienko *et al.* 2009; Kröner *et al.* 2015). Subduction of the southern PAO initiated later; the earliest SSZ-type ophiolites at 572–512 Ma (Kröner *et al.* 2007; Ryazantsev *et al.* 2009; Xu *et al.* 2012; Yang *et al.* 2012*a*; Liu *et al.* 2020), island-arc plutons at 572–495 Ma (Kröner *et al.* 2007; Alexeiev *et al.* 2011; Konopelko *et al.* 2012, 2021; Xu *et al.* 2012, 2013*b*; Ren *et al.* 2014; Zheng *et al.* 2019) and subduction-related metamorphic rocks at 509–458 Ma (Zhang, 1997; Tagiri *et al.* 2010; Alexeiev *et al.* 2011; Meyer *et al.* 2013; Konopelko & Klemd, 2016; Liu *et al.* 2016) in Kazakhstan–Kyrgyzstan Northern Tianshan and West Junggar region of China. The evidence of Ediacaran subduction has only been published more recently (Zheng *et al.* 2019; Liu *et al.* 2020); it is therefore necessary to further explore the initial subduction of the southern PAO.

The West Junggar region, northwestern China, is located in the southwestern part of the CAOB, and its accretionary process was closely related to the subduction of the Junggar Ocean, an important southern branch of the PAO (Fig. 1b; Han *et al.* 2006, 2010; Windley *et al.*

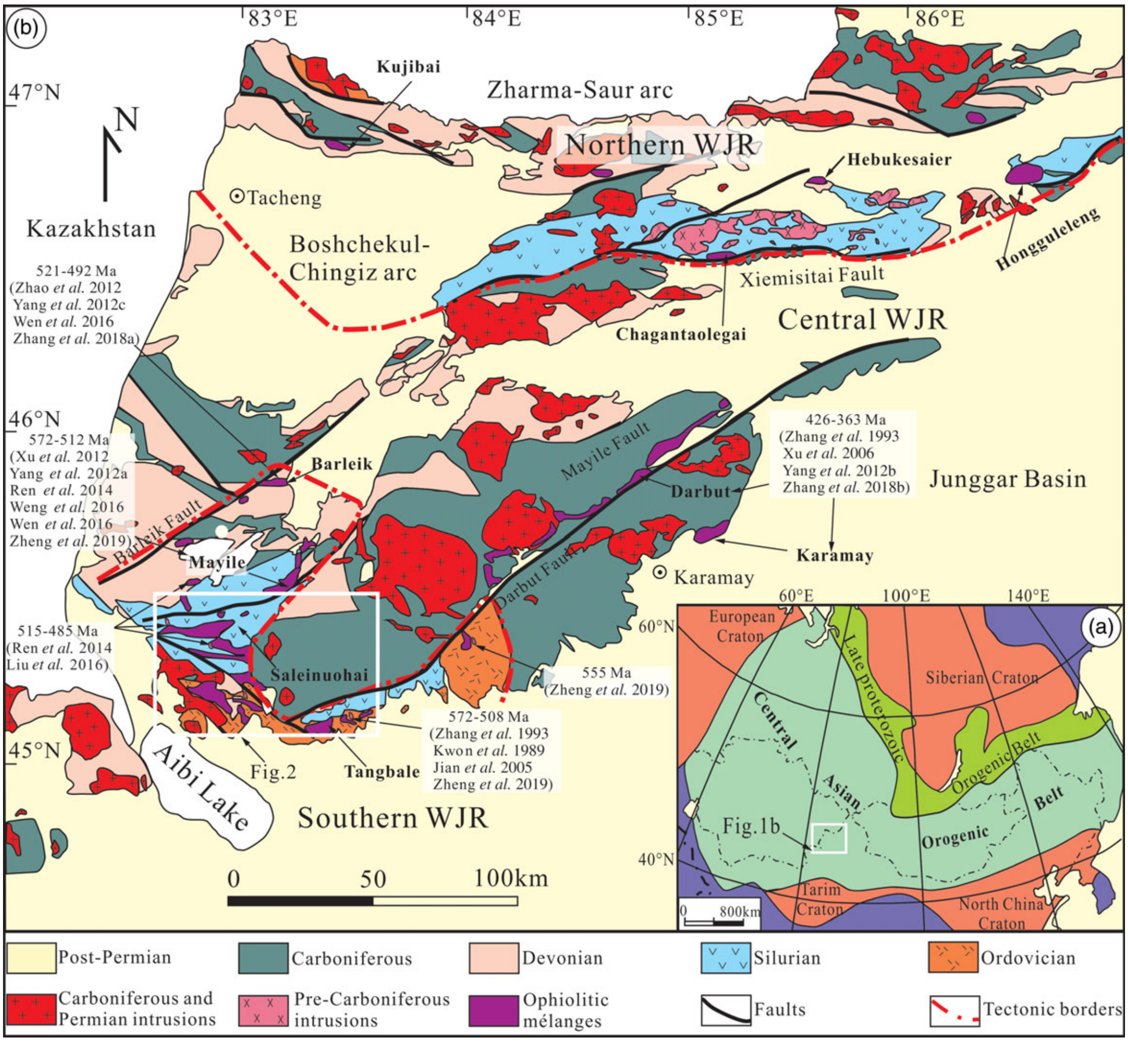

Fig. 1. (Colour online) (a) Tectonic division of the CAOB (modified from Han *et al.* 2010) with the approximate location of (b) shown in inset. (b) Tectonic map of the West Junggar region (modified from BGMRXUAR, 1993) with the approximate location of Figure 2. WJR – West Junggar region.

2007; Xiao *et al.* 2008). The Barleik–Mayile–Tangbale accretionary complexes in southern West Junggar are thought to represent the earliest part related to subduction of the Junggar Ocean (Liu *et al.* 2020), with the oldest subduction-related amphibolite of 504 Ma and blueschist of 502 Ma (Liu *et al.* 2016), SSZ-type gabbro of 572 Ma (Yang *et al.* 2012*a*; Liu *et al.* 2020) and island-arc diorite of 572 Ma (Zheng *et al.* 2019), suggesting the initial intra-oceanic subduction of the Junggar Ocean during the Ediacaran Period (Zheng *et al.* 2019; Liu *et al.* 2020). However, there is no consensus about the subduction process and polarity, with possible S-directed (Liu *et al.* 2016; Wen *et al.* 2016; Zhang *et al.* 2018*b*) or N-directed (Choulet *et al.* 2016) subduction, which would result in three isolated intra-oceanic arcs (Xu *et al.* 2012, 2013*b*; Ren *et al.* 2014) or one single intra-oceanic arc (Choulet *et al.* 2016; Liu *et al.* 2016; Wen *et al.* 2016; Zhang *et al.* 2018*b*).

In this paper, we present new whole-rock chemical data and zircon U–Pb ages from four adakitic and two non-adakitic igneous rocks as tectonic blocks in the Barleik–Mayile–Tangbale accretionary complexes, and one gabbro enclave in an adakitic block in order to further discuss the initial subduction and evolution of the Junggar Ocean during Ediacaran–Cambrian time.

2. Geological background

The West Junggar region is usually divided into northern, central and southern parts (Fig. 1b; Choulet *et al.* 2012; Liu *et al.* 2020). The northern West Junggar region is characterized by the E–W-striking Zharma–Saur arc in the north and Boshchekul–Chingiz arc in the south, separated by the Kujibai–Hebukesaier–Hongguleleng ophiolitic mélange belt (Chen *et al.* 2010, 2015; Yang *et al.* 2019*b*). The Zharma–Saur arc may be traced for up to *c.* 600 km from northeastern Kazakhstan to northwestern China and is mainly composed of Late Devonian – Early Carboniferous arc igneous rocks, which was formed by S-wards subduction of the Irtysh–Zaisan Ocean, another southern branch of the PAO (Fig. 1b; Windley *et al.* 2007; Chen *et al.* 2010, 2015). The Boshchekul–Chingiz arc (Fig. 1b) extends W-wards to the Boshchekul region in central Kazakhstan and is characterized by the Cambrian – Early Devonian arc igneous rocks (Chen *et al.* 2010; Xiao *et al.* 2015) related to either N-wards subduction of the Junggar Ocean (Choulet *et al.* 2012; Chen *et al.* 2015) or S-wards subduction of the Irtysh–Zaisan ocean (Shen *et al.* 2012; Yin *et al.* 2015). The Kujibai–Hebukesaier–Hongguleleng ophiolitic mélange belt comprises gabbros and basalts with normal mid-ocean-ridge basalt (N-MORB) affinities (Du & Chen, 2017; Yang *et al.* 2019*b*) and island-arc tholeiitic diabases and basalts (She *et al.* 2016; Liu *et al.* 2020). The gabbros and plagiogranite yield zircon U–Pb ages of 515–472 Ma (She *et al.* 2016; Du & Chen, 2017; Yang *et al.* 2019*b*), implying the presence of a Cambrian–Ordovician ocean basin (Du & Chen, 2017; Yang *et al.* 2019*b*) or back-arc basin (She *et al.* 2016) between the Zharma–Saur and Boshchekul–Chingiz arcs. Both arcs and intervening ophiolitic mélange belt were intruded by Late Carboniferous – Permian plutons (Fig. 1b; Chen *et al.* 2010).

The central West Junggar region is separated from the northern West Junggar region by the Chagantaolegai ophiolitic mélange along the Xiemisitai Fault (Fig. 1b; Chen *et al.* 2015; Liu *et al.* 2020) and composed of the Devonian – Early Carboniferous subduction-related volcano-sedimentary rocks (Xu *et al.* 2013*b*), which are intruded by Upper Carboniferous – lower Permian plutons (Fig. 1b; Han *et al.* 2006). The Late Silurian – Devonian Karamay and Darbut ophiolitic mélanges are dispersed along the NE-trending faults near the NW margin of the Junggar Basin (Fig. 1b; Zhang *et al.* 2018*a*) and dominated by diverse tectonic blocks, including N-MORB, enriched mid-ocean-ridge basalt (E-MORB) and arc-like gabbros of age 426–363 Ma (Xu *et al.* 2006; Yang *et al.* 2012*b*; Zhang *et al.* 2018*b*) and Late Devonian radiolarian-bearing cherts (Zong *et al.* 2016). These blocks are considered to have been welded together during the terminative oceanic subduction (Xu *et al.* 2013*a*; Li *et al.* 2015).

The southern West Junggar region consists mainly of Ordovician–Silurian accretionary complexes (Fig. 1b; Windley *et al.* 2007; Xiao *et al.* 2008; Han *et al.* 2010), including SSZ-type ophiolitic mélanges scattered in Barleik, Mayile, Saleinuohai and Tangbale Mountains, and are unconformably overlain by Middle Devonian – Lower Carboniferous volcanic-sedimentary sequences (Ren *et al.* 2014; Wu *et al.* 2018). The accretionary complexes and overlying sequences were intruded by Late Carboniferous-Permian plutons (Xu *et al.* 2012; Ren *et al.* 2014; Liu *et al.* 2017) and crosscut by NE–SW-striking faults (Fig. 1b).

2.a. Tangbale ophiolitic mélange

The Tangbale ophiolitic mélange is distributed in the Middle Ordovician Kekeshayi Formation and unconformably overlain by the Silurian turbidites (Fig. 2; Choulet *et al.* 2012; Zheng *et al.* 2019). The mélange is characterized by various blocks in serpentinite matrix, including serpentinized peridotite, pyroxenite, basalt, gabbro, chert and blueschist (Zhang *et al.* 1993; Buckman & Aitchison, 2001; Liu *et al.* 2020). The gabbros yield a zircon U–Pb age of 531 ± 15 Ma (Jian *et al.* 2005) and a sphene Pb–Pb age of 523 ± 7 Ma (Kwon *et al.* 1989), the cherts contain Middle Ordovician radiolarians (Buckman & Aitchison, 2001) and the blueschists give sodium (Na) amphibole $^{40}Ar/^{39}Ar$ ages of 470–458 Ma (Zhang, 1997). The gabbros show SSZ affinities, but the basalts have both island-arc basalt (IAB) and ocean-island basalt (OIB) features (BK Yang, unpub. M.Sc. thesis, Chang'an University, 2011). Recently, diorites with zircon U–Pb ages of 572–555 Ma and arc affinities are thought to be related to the initial subduction of the Junggar Ocean (Zheng *et al.* 2019).

2.b. Mayile ophiolitic mélange

The Mayile ophiolitic mélange occurs in the Saleinuohai Mountain in the south and the Mayile Mountain in the north, and is surrounded by the Middle–Upper Silurian volcanic-sedimentary sequences (Figs 1b, 2; Wang *et al.* 2003; Xu *et al.* 2012). The mélange consists of serpentinized peridotite (harzburgite, lherzolite and dunite), gabbro, pyroxenite, basalt, chert, greenschist, blueschist and amphibolite blocks in serpentinite matrix (Xu *et al.* 2012; Ren *et al.* 2014; Liu *et al.* 2020). The SSZ-type gabbros yield zircon U–Pb ages of 572–512 Ma (Xu *et al.* 2012, 2013*b*; Yang *et al.* 2012*a*; Ren *et al.* 2014; Weng *et al.* 2016). By contrast, the pillow basalts with OIB affinities (Yang *et al.* 2012*a*, 2015*a*) yield zircon U–Pb ages of 437–433 Ma (Yang *et al.* 2019*a*) and may be the remnants of seamounts near an ocean ridge (Yang *et al.* 2012*a*). In addition, this mélange contains two groups of arc plutons – *c.* 510 Ma low-K tholeiitic in an immature island arc and *c.* 490 Ma medium-K calc-alkaline in a mature island arc – as the products of S-directed subduction of the Junggar Ocean (Xu *et al.* 2012; Ren *et al.* 2014; Weng *et al.* 2016).

2.c. Barleik ophiolitic mélange

The Barleik ophiolitic mélange is dispersed along the south side of the Barleik Fault, with the southernmost occurrence at Tierekehuola (Fig. 1b; Zhao *et al.* 2012; Wen *et al.* 2016; Zhang *et al.* 2018*a*). The mélange consists of various blocks, including peridotite, clinopyroxenite, gabbro, pillow lava, greenschist, blueschist, amphibolite, marble, and quartzite (Xu *et al.* 2012; Zhao *et al.* 2012; Liu *et al.* 2016). The SSZ-type gabbroic blocks yield zircon U-Pb ages of 521-502 Ma (Xu *et al.* 2012; Yang *et al.* 2012*c*; Wen *et al.* 2016; Zhang *et al.* 2018*a*) and the OIB-type pillow lavas are comparable to the seamount basalts in the Mayile ophiolitic mélange (Xu *et al.* 2012, 2013*b*, Yang *et al.* 2012*a*; Liu *et al.* 2020). In addition, a few intermediate to felsic arc plutons with zircon U–Pb ages of 509–503 Ma are also dispersed in the region (Xu *et al.* 2013*b*). The blueschist with a phengite $^{40}Ar/^{39}Ar$ age of 492 Ma, and garnet-bearing amphibolite with a rutile SIMS U–Pb age of 502 Ma and an Na-amphibole $^{40}Ar/^{39}Ar$ age of 504 Ma, represent the oldest records of subduction metamorphism of the Junggar Ocean (Liu *et al.* 2016).

3. Samples and their petrography

Six igneous tectonic blocks in the Tangbale, Saleinuohai and Tierekehuola areas were investigated (Fig. 2), and occur as isolated blocks in either serpentinites or accretionary complexes (Fig. 3). These igneous tectonic blocks and one gabbro enclave in the Tierekehuola granodiorite were sampled for whole-rock chemical analyses and zircon U–Pb dating. According to their chemical features, the igneous tectonic blocks can be divided into adakitic and non-adakitic subgroups.

3.a. Adakitic group

From south to north, the adakitic group includes Tangbale monzonite (190621-03; Fig. 3b) and Saleinuohai monzonite (190625-01; Fig. 3e), and Tierekehuola diorite (190629-01) and granodiorite (190929-07) (Fig. 3f). The Saleinuohai monzonite is grey and fine to medium-grained, and the Tangbale monzonite is dark grey and fine-grained; both are composed of plagioclase (40–50%), potassium (K) feldspar (25–30%), amphibole (20–25%) and minor quartz (< 5%) (Fig. 4b, d). The grey, fine to medium-grained diorite consists of plagioclase (*c.* 65%), amphibole (*c.* 30%), quartz (*c.* 3%) and minor accessory minerals (Fig. 4e), and the plagioclase shows a typical zoned texture (Fig. 4f). The granodiorite is reddish, has the same texture as diorite and comprises plagioclase (*c.* 50%), quartz (*c.* 30%), amphibole (*c.* 15%) and minor accessory minerals (Fig. 4g). All K-feldspar and plagioclase are partially subjected to kaolinization and/or sericitization with a turbid appearance.

https://doi.org/10.1017/S0016756821000376 Published online by Cambridge University Press

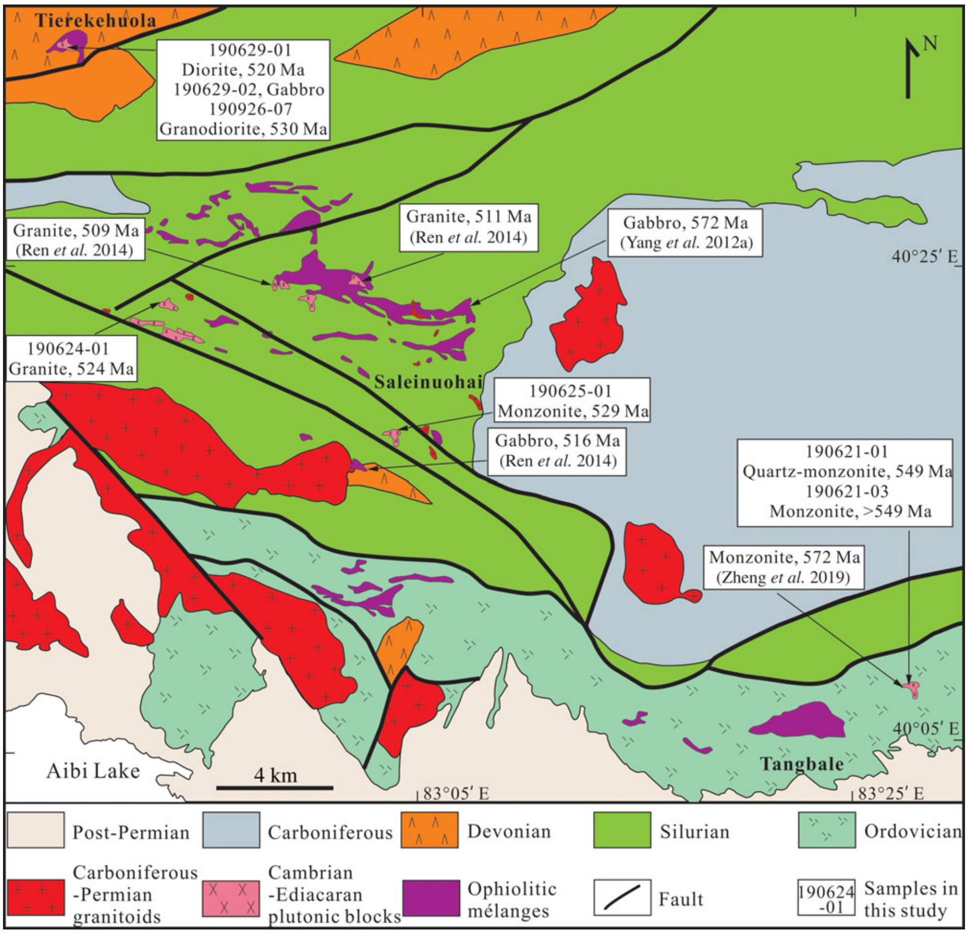

Fig. 2. (Colour online) Geological map of the study area (modified from BGMRXUAR, 1993; Ren *et al.* 2014) and sample locations.

3.b. Non-adakitic group

The non-adakitic group comprises Tangbale quartz-monzonite (190621-01; Fig. 3a) and Saleinuohai granite (190624-01; Fig. 3c, d). The non-adakitic quartz-monzonite intruded adakitic monzonite in Tangbale, which generates a chilled border on non-adakitic quartz-monzonite and a baked border on adakitic monzonite (Fig. 3b). The quartz-monzonite is reddish and fine- to medium-grained and consists of plagioclase (*c.* 40%), K-feldspar (*c.* 30%), amphibole (*c.* 15%), quartz (*c.* 10%) and minor accessory minerals (Fig. 4a). The granite is flesh pink in colour and fine- to medium-grained, with a mineral assemblage of plagioclase (*c.* 45%), K-feldspar (*c.* 30%), quartz (*c.* 20%) and minor accessory minerals (Fig. 4c). The granite intruded the serpentinite, resulting in silication of serpentinite in the contact zone (Fig. 3c, d).

3.c. Gabbro enclave

Gabbro (190629-02) is composed of clinopyroxene (*c.* 50%), plagioclase (*c.* 30%), amphibole (*c.* 10%) and minor accessory minerals (Fig. 4h).

4. Analytical methods

4.a. Zircon U–Pb dating

The mounts for zircon U–Pb dating were prepared at the Beijing Kuangyan Geoanalysis Laboratory Co. Ltd. Zircon grains were separated by crushing, heavy liquid and magnetic techniques, then picked out and embedded in an epoxy mount, and polished to expose about half of the grains. Cathodoluminescence (CL) images of zircons were photographed by a Tescan Mira3 Scanning Electron Microscope at the Beijing Kuangyan Geoanalysis Laboratory Co. Ltd, to reveal their internal structures. The spots with no cracks and inclusions were selected on CL, reflected and transmitted images for dating. U–Pb dating was conducted on laser ablation inductively coupled plasma mass spectrometry (LA-ICP-MS) at the Key Laboratory of Regional Geology and Mineralization, Hebei GEO University, in Shijiangzhuang. The system couples a quadrupole ICP-MS (THERMO-ICAPRQ) and 193-nm ArF Excimer laser (RESOlution-LR) with Laurin Technic S155 sample chamber and GeoStar µGISTM software. The ablation was taken under a designed condition with 29 µm laser beam spot, 3 J cm^{-2} laser energy density and 8 Hz frequency. Zircon standard 91500 and Plesovice were used as an external standard (Sláma *et al.* 2008) and a secondary standard to monitor the deviation of measurement, respectively. Concentration calibrations were carried out using NIST 610 glass as an external standard and Si as an internal standard. Isotopic ratios and element concentrations of zircons were calculated using ICP-MS software DataCal (Liu *et al.* 2010). Concordia ages and diagrams were obtained using Isoplot/Ex 4.15 (Ludwig, 2012). The common lead was corrected using Common Lead Correction (ver. 3.15), following the method of Andersen (2002). Analytical data are presented on U–Pb Concordia diagrams with 2σ errors.

https://doi.org/10.1017/S0016756821000376 Published online by Cambridge University Press

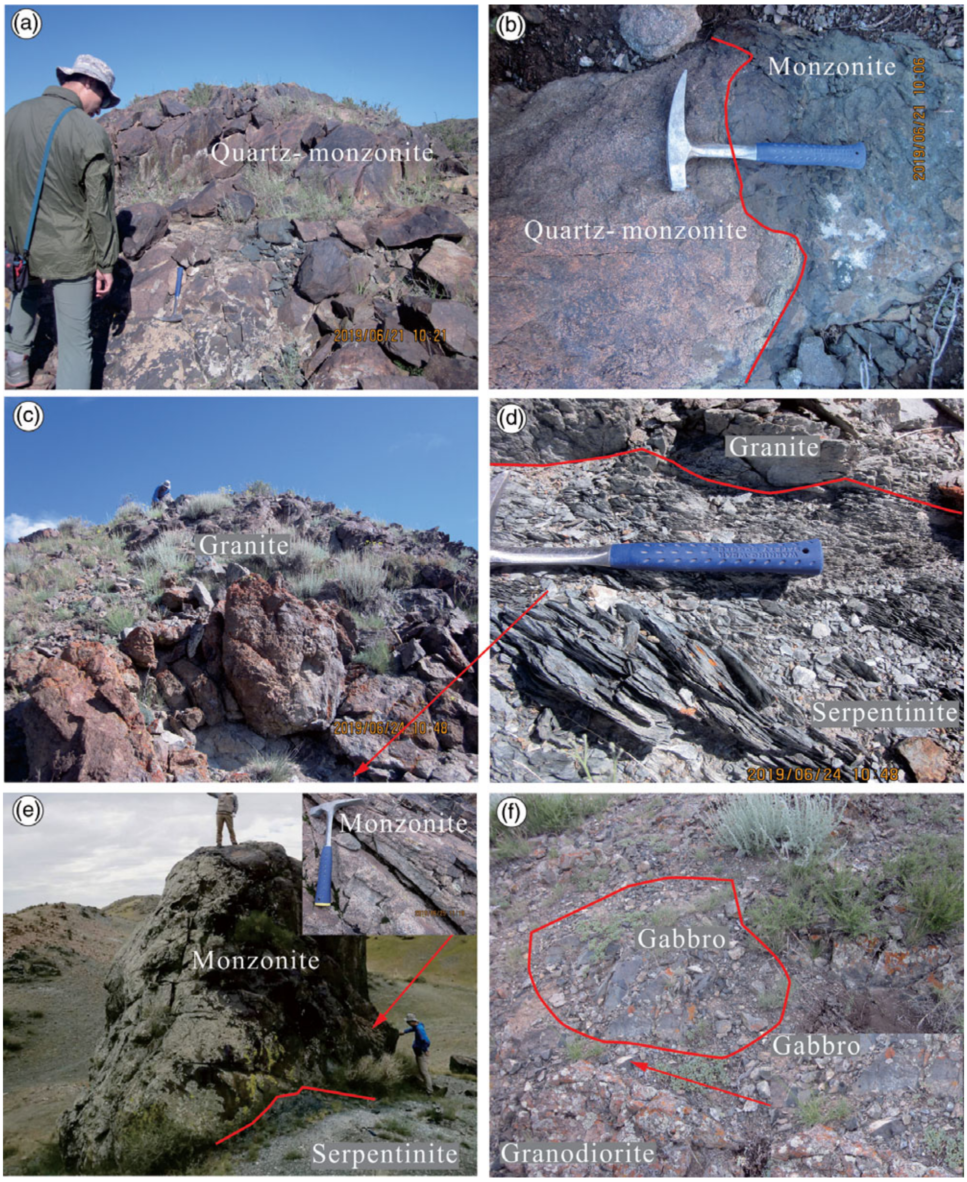

Fig. 3. (Colour online) Field photographs showing (a) Tangbale quartz-monzonite; (b) the relationship between quartz-monzonite and monzonite in Tangbale; the relationship between granite and serpentinite in the Saleinuohai (c, d); (e) Saleinuohai monzonite; and (f) granodiorite and gabbro enclave in the Tierekehuola.

4.b. Major- and trace-element compositions

Rock samples were carefully selected, crushed and then ground to less than 200 mesh (*c.* 80 μm). Major elements were analysed on ARL ADVANT' XP+, with 50 kV accelerating voltage and 50 mA accelerating current, at the Tianjin Institute of Geology and Mineral Resources of China Geological Survey. Chinese national standard samples GSR-1 and GSR-3 were used and analytical errors are better than 1%.

Trace element, including REE, analyses were performed by X series ICP-MS at the Tianjin Institute of Geology and Mineral Resources of China Geological Survey. For analyses, about 50 mg sample powder was dissolved in a mixture of HF and HNO_3 (2:1) in a screw-top Teflon beaker (Savillex) for 1 day at *c.* 190°C. After evaporation, the sample was refluxed in HNO_3 and dried twice, and finally re-dissolved in HNO_3. The procedure was repeated until complete dissolution. The data quality was monitored by five standard reference materials: AGV-2, BCR-2, BHVO-2, BIR-1 and DNC-1. The analytical errors are 1–10% for trace elements, depending on the concentrations.

5. Results

5.a. Zircon U–Pb ages

Zircons from five igneous rocks were selected for LA-ICP-MS dating. A summary of age data is given in Table 1, and all the data are presented in online Supplementary Table S1 (available at http://journals.cambridge.org/geo) and representative CL images of zircon grains are shown in Figure 5. The zircon grains are colourless, transparent, euhedral and prismatic in shape, with 20–200 μm in width and 30–200 μm in length (Fig. 5), and most grains show well-developed oscillatory zones. Analyses with < 95% concordance are excluded from age calculations.

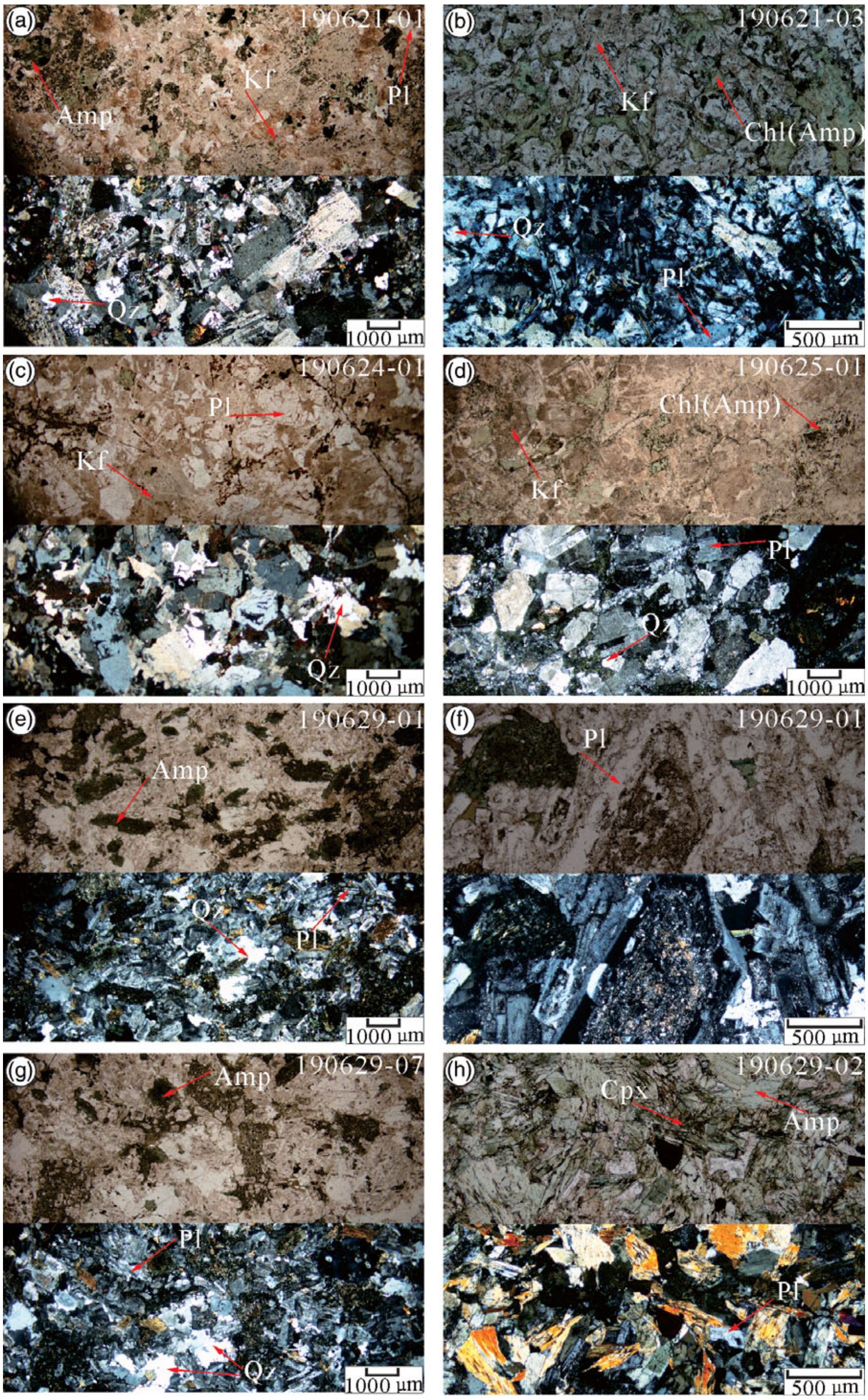

Fig. 4. (Colour online) Representative plane-polarized (upper part) and cross-polarized (lower part) photomicrographs of (a) Tangbale quartz-monzonite, (b) Tangbale monzonite, (c) Saleinuohai granite, (d) Saleinuohai monzonite, (e) Tierekehuola diorite, (f) plagioclase zoning in Tierekehuola diorite, (g) Tierekehuola granodiorite and (h) Tierekehuola gabbro. Amp – amphibole; Chl – chlorite; Cpx – clinopyroxene; Kf – potassium feldspar; Pl – plagioclase; Qz – quartz.

5.a.1. Adakitic group

A total of 24 zircon grains were dated for Saleinuohai monzonite (190625-01); their U and Th concentrations are in the ranges of 121–421 and 44–514 ppm, respectively, with Th/U ratios of 0.37–1.22. With the exception of one grain with a younger $^{206}Pb/^{238}U$ age of 510 ± 8 Ma (No.18), the remaining 23 grains yield a concordant age of 529 ± 2 Ma (MSWD = 0.51; Fig. 6c).

For Tierekehuola diorite (190629-01), the dated 26 zircon grains have U and Th concentrations of 118–467 and 30–192 ppm, respectively, with Th/U ratios of 0.21–0.48. Spot 1 gives a younger $^{206}Pb/^{238}U$ age of 512 ± 6 Ma, and spots 13 and 17 give older $^{206}Pb/^{238}U$ ages of 535 ± 6 and 535 ± 9 Ma, respectively. The other 23 grains yield a concordant age of 520 ± 1 Ma (MSWD = 0.41; Fig. 6d).

https://doi.org/10.1017/S0016756821000376 Published online by Cambridge University Press

Table 1. Summary of zircon information. Con – concordant.

Rock type	Sample no.	Length *L* (μm)	Width *W* (μm)	*L*/*W*	Th (ppm)	U (ppm)	Th/U	Age (Ma)		
								Min	Max	Con
Quartz monzonite	190621-01	50–100	30–50	1–2	120–1465	164–1462	0.62–1.38	513	571	549
Granite	190624-01	30–100	20–80	1–2	38–1334	103–2198	0.34–0.65	523	541	524
Monzonite	190625-01	100–150	50–100	1–3	44–514	121–421	0.37–1.22	505	533	529
Diorite	190629-01	150–200	100–200	1–2	30–192	118–467	0.21–0.48	512	535	520
Granodiorite	190629-07	80–200	80–100	1–3	27–158	122–442	0.21–0.42	511	532	530

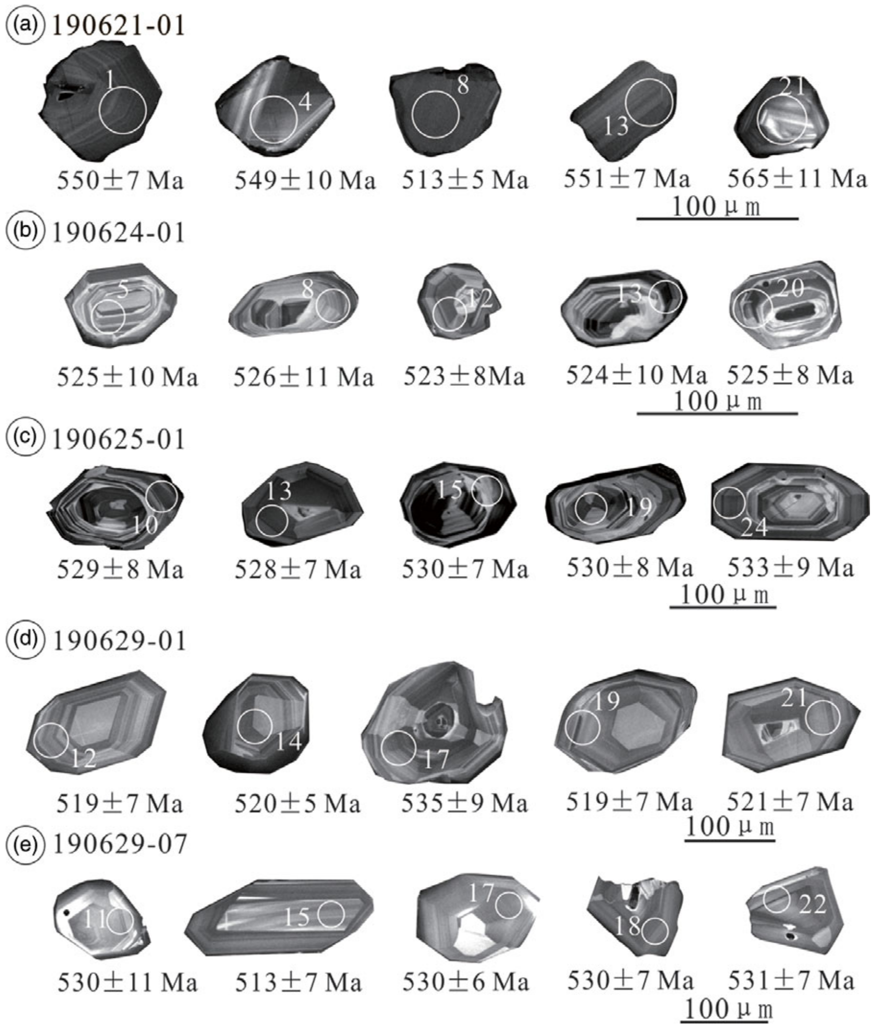

Fig. 5. (Colour online) Representative cathodoluminescence (CL) images of zircon grains and $^{206}Pb/^{238}U$ ages.

A total of 21 analyses for Tierekehuola granodiorite (190629-07) are valid and their U and Th concentrations vary over 122–421 and 27–158 ppm, respectively, with Th/U ratios of 0.21–0.42. With the exception of one grain with a younger $^{206}Pb/^{238}U$ age of 513 ± 7 Ma (No.15), the other 20 gains yield a concordant age of 530 ± 2 Ma (MSWD = 0.21).

The concordant ages above show that the adakitic rocks were formed at 530–520 Ma.

5.a.2. Non-adakitic group

A total of 21 valid analyses from Tangbale quartz-monzonite (190621-01) show large variations in U and Th concentrations, varying over 164–1462 and 120–1465 ppm, respectively, with Th/U ratios of 0.62–1.38. Two grains give younger $^{206}Pb/^{238}U$ ages of 513 ± 5 (No. 8) and 514 ± 4 Ma (No. 15), and three grains have older $^{206}Pb/^{238}U$ ages of 571 ± 5 Ma (No. 9), 570 ± 8 (No. 11) and 565 ± 5 (No. 21). The other 16 grains yield a concordant age of

https://doi.org/10.1017/S0016756821000376 Published online by Cambridge University Press

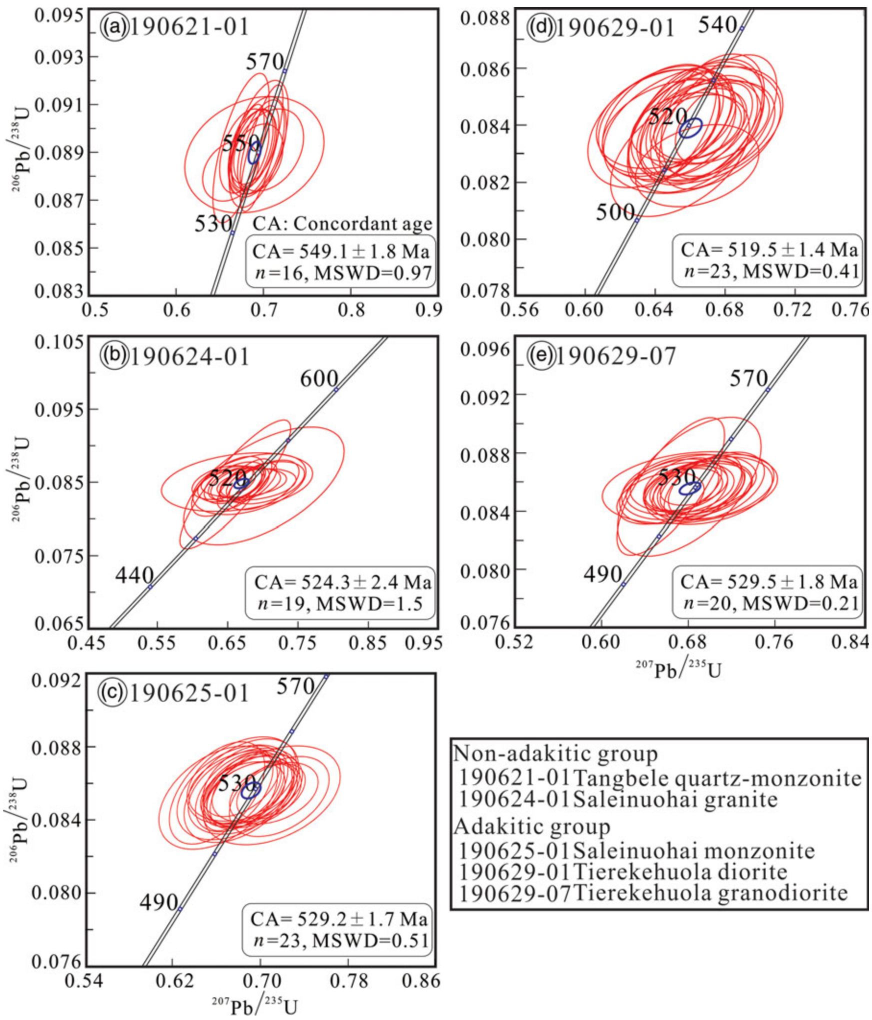

Fig. 6. (Colour online) U–Pb concordia diagrams for (a) Tangbale quartz-monzonite, (b) Saleinuohai granite, (c) Saleinuohai monzonite, (d) Tierekehuola diorite and (e) Tierekehuola granodiorite. MSWD – mean square of weighted deviates. Zircon U–Pb data are provided in online Supplementary Table S1.

549 ± 2 Ma (MSWD = 0.97; Fig. 6a), which is considered as the crystallization age of the block.

For Saleinuohai granite (190624-01), 20 zircon grains were dated. They have U and Th concentrations of 103–2198 and 38–1334 ppm, respectively, with Th/U ratios of 0.34–0.65. With the exception of one analysis with an older $^{206}Pb/^{238}U$ of 541 ± 9 Ma (No.16), the other 19 grains yield a concordant age of 524 ± 2 Ma (MSWD = 0.15; Fig. 6b), which represents the crystallization age of the granite.

5.b. Whole-rock elemental chemistry

The chemical compositions of four adakitic and two non-adakitic igneous rocks and one gabbro enclave are presented in Table 2.

5.b.1. Adakitic group

The samples have 58.90–64.51 wt% SiO_2, 15.11–17.66 wt% Al_2O_3, 2.65–4.72 wt% MgO and 0.45–1.57 wt% K_2O, with Mg no. = 46–60 and K_2O/Na_2O = 0.17–0.33, showing the compositional features of low-K tholeiitic and calc-alkaline series (Fig. 7c). They are metaluminous to peraluminous (Fig. 7b), with A/CNK (Al_2O_3/ (CaO + Na_2O + K_2O) mol%) and A/NK (Al_2O_3/ (Na_2O + K_2O) mol%) values ranging over 0.88–1.07 and 1.28–2.78, respectively.

The adakitic group is characterized by relatively high Sr (300–663 ppm) and low Y (6.68–11.2 ppm) and heavy rare earth elements (HREEs) (Yb = 0.74–1.63 ppm), with Sr/Y = 40–84 (Table 2). They have relatively low REE concentrations of 41.59–69.72 ppm and show light REE (LREE) enrichment ($(La/Yb)_N$ = 5.13–10.24), with slightly negative Ce (δ_{Ce} = 0.84–0.96) and positive Eu anomalies (δ_{Eu} = 1.06–1.26) (Fig. 8a), and they show similar large-ion lithophile element (LILE) enrichment and Nb, Ta, Zr and Hf depletion, with varying Ti depletion (Fig. 8b).

5.b.2. Non-adakitic group

The quartz-monzonite has 61.54–63.10 wt% SiO_2, 15.33–15.76 wt% Al_2O_3, 1.80–1.97 wt% MgO and 3.87–3.88 wt% K_2O, with Mg no. = 36–40 and K_2O/Na_2O = 0.92–0.94. It is high-K calc-alkaline series (Fig. 7c) and metaluminous (A/CNK = 0.91–0.92; A/NK = 1.40–1.41; Fig. 7b). By contrast, the granite is high in SiO_2 (71.29–77.42 wt%), low in Al_2O_3 (12.36–12.44 wt%), MgO (0.88–1.06 wt%) and K_2O/Na_2O = 0.63–0.77, with similar Mg no. = 38–41 and K_2O (3.02–3.41 wt%) to the quartz-monzonite. It belongs to calc-alkaline series (Fig. 7c) and is peraluminous (A/CNK = 1.06; A/NK = 1. 13; Fig. 7b).

https://doi.org/10.1017/S0016756821000376 Published online by Cambridge University Press

Table 2. Major (wt%) and trace element (ppm) results of the igneous rocks

	Non-adakitic group					Adakitic group										
	190621-01			190624-01		190621-03		190625-01			190629-01			190629-07		190629-02	
	Quartz monzonite			Granite		Monzonite		Monzonite			Diorite			Granodiorite		Gabbro enclave	
	a	b	c	a	b	a	b	a	b	c	a	b	c	a	b	a	b
SiO_2	63.10	62.75	61.54	74.40	74.41	58.90	59.77	57.61	57.97	58.57	60.22	60.25	62.81	63.43	64.51	49.80	50.08
TiO_2	0.51	0.54	0.56	0.32	0.30	0.68	0.70	0.54	0.53	0.47	0.44	0.45	0.42	0.40	0.33	0.51	0.53
Al_2O_3	15.33	15.47	15.76	12.44	12.36	16.71	16.45	17.66	16.94	16.97	16.64	16.93	16.55	15.11	15.43	9.17	9.69
$Fe_2O_3^T$	5.94	6.03	6.70	2.69	2.80	6.41	6.18	5.92	6.13	6.02	7.70	7.47	6.26	6.42	6.21	11.46	10.94
MnO	0.10	0.10	0.10	0.07	0.09	0.11	0.09	0.12	0.12	0.08	0.15	0.14	0.12	0.11	0.10	0.21	0.20
MgO	1.97	1.80	1.88	1.06	0.88	4.52	4.32	4.24	4.44	4.72	3.29	3.17	2.65	2.78	2.75	15.11	14.81
CaO	3.15	3.07	3.34	0.40	0.39	3.25	3.52	3.60	3.19	3.17	5.36	5.43	4.39	6.49	5.86	9.82	9.45
Na_2O	4.13	4.16	4.24	4.74	4.39	5.98	6.41	7.14	7.11	6.91	3.33	3.34	3.74	2.91	3.34	1.71	1.81
K_2O	3.87	3.87	3.88	3.02	3.41	1.34	1.14	1.47	1.42	1.57	1.08	1.05	1.25	0.59	0.45	0.31	0.35
P_2O_5	0.27	0.24	0.24	0.06	0.06	0.17	0.18	0.16	0.17	0.15	0.16	0.17	0.14	0.16	0.16	0.16	0.18
LOI	1.62	1.98	1.76	0.82	0.91	1.94	1.23	1.55	1.79	1.38	1.61	1.60	1.68	1.61	0.86	1.74	1.95
Total	99.99	100.01	100.00	100.01	99.99	100.01	99.99	100.01	100.01	100.00	99.98	100.00	100.01	100.01	100.00	100.00	99.99
Mg no.	40	37	36	41	38	58	58	58	59	60	46	46	46	46	47	72	73
A/NK	1.40	1.40	1.41	1.13	1.13	1.48	1.40	1.32	1.28	1.31	2.50	2.55	2.21	2.78	2.58	—	—
A/CNK	0.92	0.93	0.91	1.06	1.06	0.97	0.90	0.89	0.89	0.91	1.02	1.03	1.07	0.88	0.93	—	—
Sc	12.50	14.10	14.80	10.60	11.55	13.20	17.51	16.40	18.80	14.27	22.02	19.30	15.20	17.06	15.32	36.11	35.43
V	95.40	118	122	13.20	12.60	113	121	122	128	140	184	173	138	138	134	236	246
Cr	8.33	9.23	9.54	1.30	0.80	89.90	96.50	93.27	97.40	94.35	8.02	11.80	5.49	7.14	6.75	1360	1120
Co	10.71	11.22	11.40	2.52	2.22	17.01	17.80	9.78	8.21	8.33	16.20	15.03	13.06	13.50	13.40	48.60	45.40
Ni	6.11	7.92	7.52	1.15	0.83	71.90	75.04	73.41	79.69	78.89	7.42	6.97	5.20	5.96	5.57	288	231
Cu	40.21	28.11	23.84	6.08	3.29	48.93	48.20	41.51	30.80	50.24	31.90	93.22	46.84	4.69	3.69	12.09	52.80
Zn	62.41	57.40	59.12	60.22	38.51	65.03	64.10	71.60	71.23	76.31	71.04	60.21	55.33	36.41	34.73	92.33	90.52
Ga	15.31	15.03	15.21	11.94	10.91	16.32	16.71	13.05	13.41	14.56	15.30	14.30	13.11	11.40	10.74	10.80	10.53
Rb	33.80	27.90	31.01	20.02	24.90	8.85	8.34	5.80	6.33	6.01	11.70	8.76	8.36	5.46	4.62	3.69	3.95
Sr	212	330	360	150	158	300	591	470	498	488	520	473	463	660	584	149	214
Y	21.30	22.03	22.70	16.80	13.20	6.68	7.03	6.20	8.40	7.20	12.20	11.80	8.68	9.82	10.10	8.07	8.77
Zr	132	146	143	104	104	56.51	55.82	63.52	61.31	64.21	60.55	65.20	52.72	48.54	44.53	29.23	34.91
Nb	4.31	3.81	3.82	3.87	3.59	1.68	1.67	1.88	1.98	1.99	1.64	1.56	1.64	1.40	1.13	0.91	1.06
Cs	0.33	0.12	0.11	6.94	7.48	0.99	0.07	0.16	0.09	0.11	1.22	1.01	1.29	0.19	0.23	0.40	0.39

(*Continued*)

https://doi.org/10.1017/S0016756821000376 Published online by Cambridge University Press

Table 2. (*Continued*)

	Non-adakitic group					Adakitic group											
	190621-01			190624-01		190621-03		190625-01			190629-01			190629-07		190629-02	
	Quartz monzonite			Granite		Monzonite		Monzonite			Diorite			Granodiorite		Gabbro enclave	
	a	b	c	a	b	a	b	a	b	c	a	b	c	a	b	a	b
Ba	862	866	904	1220	1180	554	326	413	620	601	1010	858	912	1100	780	239	228
Hf	4.25	4.43	4.54	3.60	3.66	2.05	2.02	2.12	2.07	2.18	2.05	2.16	1.70	1.63	1.48	1.09	1.27
Ta	0.24	0.21	0.21	0.23	0.22	0.13	0.13	0.14	0.12	0.15	0.10	0.10	0.11	0.08	0.07	0.05	0.06
Pb	3.39	4.64	4.74	7.22	3.83	2.07	4.11	2.01	3.07	4.21	2.07	1.85	1.90	1.44	1.09	0.42	0.61
Th	3.69	2.88	2.94	2.54	2.42	0.89	0.97	0.99	1.07	1.21	1.90	1.82	1.68	1.63	1.19	0.94	1.13
U	1.82	1.40	1.40	1.18	1.44	0.40	0.45	0.59	0.81	0.76	0.81	0.85	0.50	0.79	0.78	0.37	0.53
La	28.70	23.50	23.40	23.70	14.60	6.46	7.53	8.20	7.90	8.50	12.01	11.02	8.08	12.03	9.76	9.55	9.32
Ce	63.50	41.90	51.40	46.01	27.70	14.50	15.10	15.50	16.90	18.91	23.30	21.70	14.50	22.90	20.40	20.02	19.60
Pr	8.68	6.78	6.77	6.72	4.43	2.14	2.43	2.70	3.14	3.55	3.66	3.44	2.59	3.50	3.04	3.59	3.62
Nd	33.71	27.82	27.81	27.50	18.41	9.63	10.90	10.13	10.81	11.40	15.80	14.93	11.22	14.60	13.41	16.41	16.82
Sm	6.25	5.66	5.80	5.44	3.86	2.11	2.35	2.55	2.49	2.63	3.38	3.35	2.45	3.04	2.96	3.54	3.76
Eu	1.68	1.51	1.55	1.17	1.03	0.81	0.81	0.88	0.89	0.88	1.21	1.12	0.97	1.13	1.04	1.01	1.04
Gd	5.40	4.95	5.09	4.48	3.19	1.83	1.97	1.76	1.88	1.98	3.02	2.97	2.17	2.79	2.66	2.81	2.94
Tb	0.83	0.81	0.83	0.72	0.54	0.29	0.31	0.32	0.33	0.36	0.48	0.46	0.33	0.40	0.40	0.40	0.43
Dy	4.58	4.50	4.64	4.04	3.14	1.55	1.63	1.41	1.62	1.66	2.66	2.57	1.85	2.16	2.18	2.01	2.19
Ho	0.90	0.90	0.92	0.79	0.63	0.29	0.30	0.31	0.30	0.31	0.52	0.51	0.37	0.42	0.42	0.36	0.40
Er	2.72	2.69	2.76	2.39	1.98	0.80	0.84	0.89	0.88	0.89	1.56	1.48	1.08	1.22	1.24	1.02	1.11
Tm	0.43	0.43	0.44	0.38	0.33	0.12	0.12	0.13	0.12	0.13	0.24	0.23	0.17	0.18	0.19	0.14	0.16
Yb	2.92	2.84	2.89	2.49	2.32	0.74	0.76	0.82	0.81	0.83	1.63	1.54	1.13	1.24	1.26	0.91	1.01
Lu	0.47	0.46	0.46	0.40	0.38	0.12	0.12	0.13	0.13	0.13	0.26	0.25	0.19	0.20	0.20	0.14	0.16
REE	160.76	124.73	134.75	126.22	82.53	41.59	45.17	41.70	48.10	52.16	69.72	65.52	47.08	65.78	59.15	61.86	62.54
Nb/La	0.15	0.16	0.16	0.16	0.25	0.26	0.22	0.22	0.25	0.23	0.14	0.14	0.20	0.12	0.12	0.10	0.11
La_N/Yb_N	7.05	5.94	5.81	6.83	4.52	8.73	9.91	10.01	9.75	10.24	5.28	5.13	5.13	6.94	5.56	7.53	6.62
Eu*	0.86	0.85	0.85	0.70	0.87	1.23	1.12	1.20	1.23	1.13	1.14	1.06	1.26	1.17	1.11	0.95	0.92

Mg no. = 100 × (MgO/40.3)/[MgO/40.3 + $(0.9\times Fe_2O_3{}^T/71.85)$]; Eu* = $2Eu_N/(Sm_N + Gd_N)$.

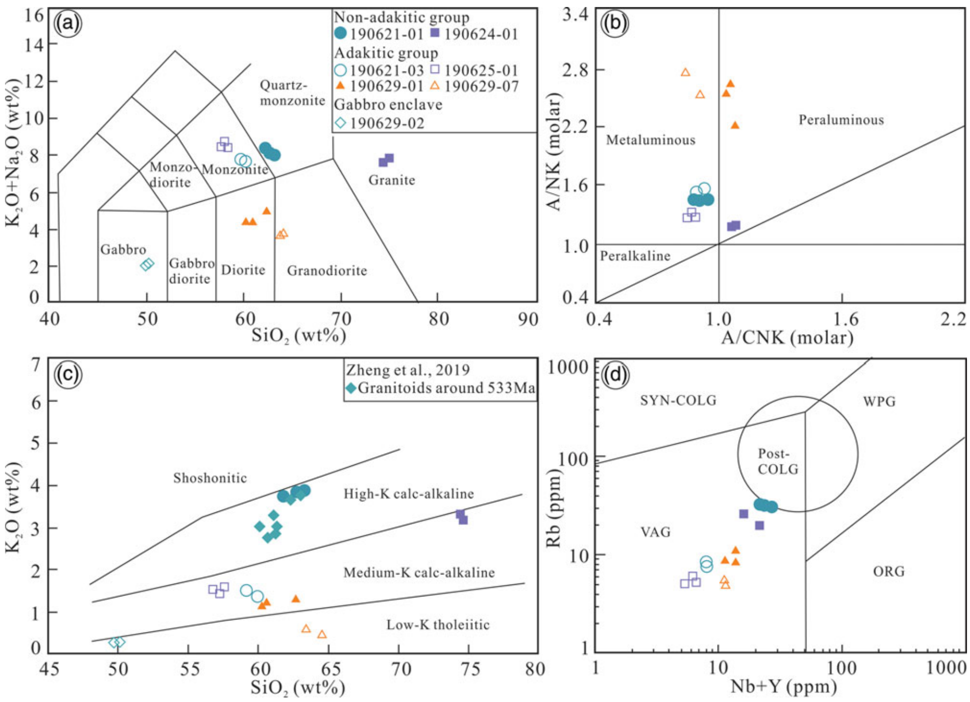

Fig. 7. (Colour online) (a) TAS diagram for the adakitic and non-adakitic rocks and gabbro enclave (after Middlemost *et al.* 1994); (b) A/NK versus A/CNK diagram showing that the adakitic and non-adakitic rocks are metaluminous to peraluminous (after Maniar & Piccoli, 1989); (c) K_2O versus SiO_2 diagram for the adakitic and non-adakitic rocks and gabbro (after Peccerillo & Taylor, 1976); and (d) Rb versus (Nb+Y) diagram showing that the adakitic and non-adakitic rocks are in VAG field (after Pearce *et al.* 1984). ORG – oceanic ridge granites; Post-COLG – post-collisional granites; Syn-COLG – syn-collisional granite; VAG – volcanic arc granites; WPG – within-plate granites.

The quartz-monzonite and granite have similar trace-element features. They are characterized by higher Y (13.2–22.7 ppm) and HREE (Yb = 2.32–2.92 ppm), lower Sr/Y (9–16) than the adakitic group and total REE concentrations of 82.5–160.8 ppm (Table 2). The non-adakitic group has similar REE and trace-element patterns as the adakitic group, but they have negative Eu anomalies (δ_{Eu} = 0.70–0.87), less LREE enrichment ($(La/Yb)_N$ = 4.52–7.05) and stronger Ti depletion (Fig. 8c, d).

5.b.3. Gabbro enclave

The gabbro is characterized by low Al_2O_3 (9.17–9.69 wt%) and K_2O (0.31–0.35 wt%) and high MgO (14.81–15.11 wt%), with Mg no. = 72–73 and K_2O/Na_2O = 0.18–0.19. It has low REE contents of 61.9–62.5 ppm, with slightly negative Eu (δ_{Eu} = 0.92–0.95) and Ce (δ_{Ce} = 0.83–0.85) anomalies (Fig. 8c) and fractionated REE patterns ($(La/Yb)_N$ = 6.62–7.53). The gabbro enclave contains relatively high Cr (1120–1360 ppm), Ni (231–288 ppm), Co (45–48 ppm) and V (236–246 ppm) concentrations, and shows significant Nb, Ta, Zr, Hf and Ti depletion and Ba and U enrichment (Fig. 8d).

6. Discussion

The adakitic and non-adakitic igneous rocks are usually small in size (area of 50–600 m^2) and occur mostly as isolated blocks, but the Tangbale adakitic monzonite is intruded by the Tangbale non-adakitic quartz-monzonite at 549 Ma, implying that the former was formed earlier. Similarly, the Saleinuohai adakitic monzonite was formed at 529 Ma, also earlier than the Saleinuohai non-adakitic granite at 524 Ma, but the emplacement of the adakitic granodiorite in Tierekehuola at 530 Ma was followed by the adakitic diorite at 520 Ma. In addition, the gabbro enclave was trapped by the adakitic granodiorite at 530 Ma. Locally, the adakitic rocks were formed earlier than the non-adakitic ones. Spatially, the igneous rocks show a progressively N-wards younger trend from Tangbale to Tierekehuola.

6.a. Petrogenesis

6.a.1. Adakitic group

These rocks are characterized by SiO_2 (57.61–64.51 wt%) and Al_2O_3 (15.11–17.66 wt%), with Mg no. = 46–60, relatively high Sr (300–663 ppm), Sr/Y (40–84) and Cr/Ni (1.06–1.69), and relatively low HREE (Yb = 0.74–1.63 ppm) and Y (6.68–12.2 ppm), which are typical of adakite (Figs 9a, 10c, d; Defant & Drummond, 1990) and high-SiO_2 adakite (Martin *et al.* 2005; Konopelko *et al.* 2021). The adakite may be generated by (1) partial melting of subducted oceanic crust with or without contribution from mantle wedge (Defant & Drummond, 1990; Martin *et al.* 2005; Zhu *et al.* 2009; Wu *et al.* 2015); (2) assimilation and fractional crystallization of basaltic magma (Defant & Drummond, 1990; Zhou *et al.* 2006); (3) partial melting of thickened or delaminated lower crust (Petford & Atherton, 1996; Ernst, 2010); or (4) mixing of felsic and basaltic magmas (Streck *et al.* 2007).

For the Ediacaran–Cambrian adakitic rocks in southern West Junggar region, their high Ni (> 5.5 ppm) and Mg no. (> 46) and low K_2O (< 1.5 wt%) and Rb/Sr (< 0.03) are different from those of the adakite generated by partial melting of thickened lower crust (Rapp & Watson, 1995; Skjerlie & Patiño Douce, 2002; Liu *et al.* 2018). Moreover, their REE and trace-element features, especially low Th (< 2 ppm), are not consistent with lower-crust-derived adakitic rocks (Hou *et al.* 2004; Wang *et al.* 2005; Zhou *et al.* 2006). Additionally, the adakitic rocks show no differential trends of basaltic magma, such as decreasing Mg no., Dy/Yb and Y with increasing SiO_2 (Ma *et al.* 2013), or Mg no. > 60 for mantle-derived adakites (Martin *et al.* 2005; Zhang *et al.* 2010).

https://doi.org/10.1017/S0016756821000376 Published online by Cambridge University Press

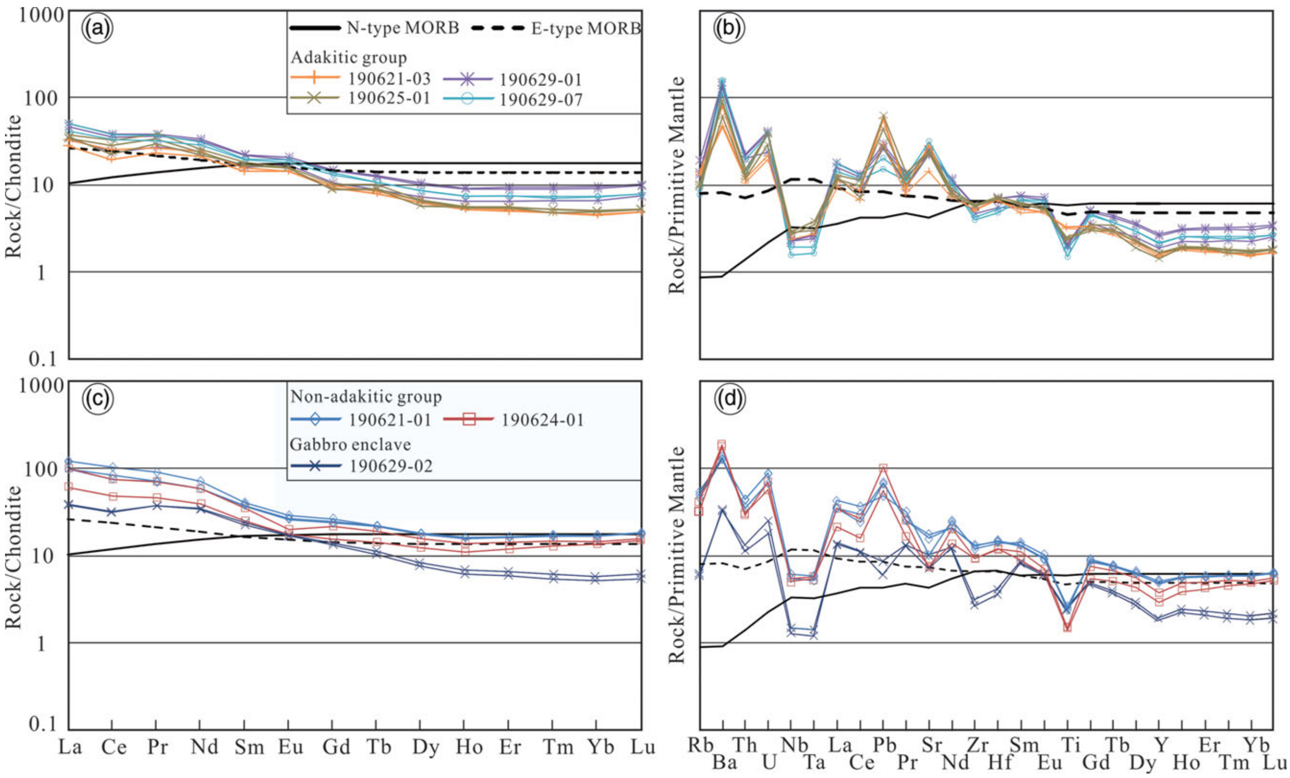

Fig. 8. (Colour online) Chondrite-normalized REE patterns and primitive-mantle-normalized trace-element spider diagrams of (a, b) the adakitic rocks, (c) the non-adakitic rocks and (d) gabbro. Chondrite, primitive mantle, N-MORB and E-MORB values are from Sun & McDonough (1989).

In addition to the similarities to those of the adakites derived from subducted oceanic crust (i.e. Mg no. > 46, Cr > 6 ppm and Ni > 5.5 ppm) (Smithies, 2000; Zhang *et al.* 2010; Ma *et al.* 2013; Liu *et al.* 2019), their low K_2O (< 1.5 wt%), relatively uniform K_2O/Na_2O (0.13–0.35) and high CaO/Al_2O_3 (0.2–0.42) resemble the oceanic-crust-derived adakites (Fig. 11) with K_2O/Na_2O (< 0.7) and high CaO/Al_2O_3 (> 0.2) (Martin *et al.* 2005; Ma *et al.* 2013; Wu *et al.* 2015; Zhang *et al.* 2019). The high-SiO_2 adakitic rocks could be derived from young subducted oceanic crust (Martin *et al.* 2005; Konopelko *et al.* 2021), similar to the Cook Island adakites derived from oceanic slab (Fig. 10a; Stern & Kilian, 1996).

The low Mg no. (< 45) adakites may result from partial melting of basalt (Rapp *et al.* 1999), but their Mg no. and Cr and Ni concentrations will increase if components from the mantle wedge were significantly incorporated into the melt derived from the subducting oceanic crust (Fig. 9a; Rapp & Watson, 1995; Tsuchiya *et al.* 2005; Wu *et al.* 2015). The interaction of the mantle wedge and slab melt might be the cause for high Mg no. (58–60), Cr (89.9–97.4 ppm) and Ni (71.9–79.7 ppm) in the Tangbale and Saleinuohai monzonites (Fig. 10b), but the Tierekehuola diorite and granodiorite were mainly formed from the slab melt, with little contribution from the mantle wedge (Fig. 10b).

The adakitic rocks show Sr enrichment and slightly positive Eu anomalies (Fig. 8), suggesting that plagioclase could not be a residual phase in the source, and their Y and HREE depletion (Fig. 8) might be caused by garnet and/or amphibole residues in the source (Defant & Kapezhinskas, 2001; Martin *et al.* 2005). The residual garnet and amphibole in the source could result in fractionated HREE patterns with Y/Yb > 10 and flat HREE patterns with Y/Yb < 10 in the melts, respectively (Ge *et al.* 2002). The adakitic rocks with Y/Yb = 7–10 might result from a residual amphibole source (Zhou *et al.* 2006; Ashraf *et al.* 2019), but the Tangbale and Saleinuohai monzonites with Y/Yb = 9–10 were derived from a minor residual garnet source that would be deeper than a residual amphibole source for the Tierekehuola diorite and granodiorite with Y/Yb = 7–8 (Fig. 10d, Zhou *et al.* 2006).

In addition, subduction-related magmas may be modified by subducted sediments and/or slab-derived fluids that are mainly composed of the seawater in the altered and cracked oceanic crust (Elburg *et al.* 2002; Wu *et al.* 2015, Bellot *et al.* 2018). The slab-derived fluids are typically enriched in Ba, Rb, Sr, U and Pb, whereas subducted sediments usually have high Th and LREE contents (Hawkesworth *et al.* 1997). The subducted sediments could result in increasing Th contents up to *c.* 20 ppm and Th/Yb ratios > 2 in subduction-related magmas, in contrast with low Th contents and Th/Yb < 1 in the magmas predominantly affected by slab-derived fluids (Nebel *et al.* 2007). Because of low Th contents (< 2 ppm) and Th/Yb ratios (< 1.3) in the adakitic rocks, the magmas might be predominantly affected by slab-derived fluids. The fluids released from subducted slab first fertilize the mantle wedge, and then the ascending melts are interacted with the mantle wedge and modified by the fluids. The slightly negative Ce anomalies of the adakites may therefore be caused by the subducted seawater (Fig. 8a; Bellot *et al.* 2018).

Overall, the adakitic rocks were mainly the partial melts of subducted oceanic crust, but the melts were modified by mantle wedge and slab-derived fluids.

6.a.2. Non-adakitic group

The Tangbale quartz-monzonite and Saleinuohai granite are calc-alkaline to high-K calc-alkaline (Fig. 7c) and metaluminous to

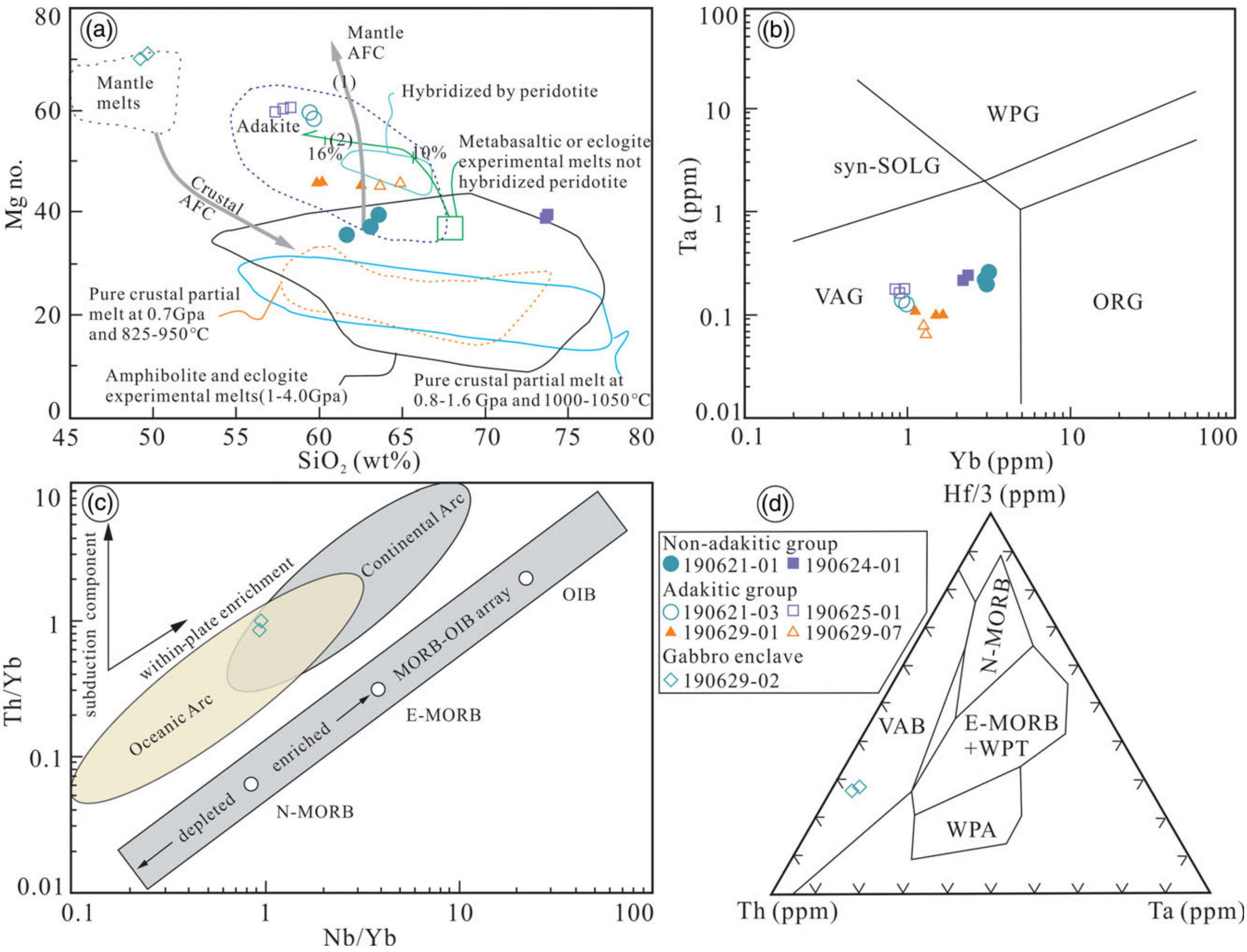

Fig. 9. (Colour online) (a) SiO_2 versus Mg no. diagram showing that gabbro plots in the field of mantle melts, and the adakitic and non-adakitic rocks plot in the field of adakite or amphibolite and eclogite experimental melts (after Cai *et al.* 2015). The field of adakite is after Wang *et al.* (2006). The field of pure crustal partial melt at 0.7 GPa and 825–950°C, amphibolite and eclogite experimental melts at 1–4 GPa and pure crustal partial melts at 0.8–1.6 GPa and 1000–1050°C are after Sen & Dunn (1994), Rapp (1995), Rapp & Watson (1995) and Sisson *et al.* (2005). The mantle AFC curves are after Stern & Kilian (1996) (1) and Rapp *et al.* (1999) (2). (b) Yb versus Ta diagram showing that the adakitic and non-adakitic rocks are in VAG field (after Pearce *et al.* 1984). (c) Nb/Yb versus Th/Yb (after Pearce, 2008). (d) Th–Hf–Ta (after Wood, 1980) diagrams showing the gabbro is likely formed as part of oceanic arc. VAB – volcanic-arc basalt; OIB – ocean-island basalt; WPT – within-plate tholeiite; WPA – within-plate alkali basalt; E-MORB – enriched mid-ocean-ridge basalt; N-MORB – normal mid-ocean-ridge basalt.

weak peraluminous (Fig. 7b), but they contain no Al-rich minerals or arc-related I-type granitoids.

The I-type granitoids in an intra-oceanic-arc system may be generated by: (1) partial melting of the middle or lower arc crust (Petford & Gallagher, 2001; Smith *et al.* 2003; Cai *et al.* 2015); (2) assimilation and fractional crystallization of mantle-derived magma (Chiaradia, 2009); or (3) mixing of crustal and mantle-derived magmas (Zhang *et al.* 2013; Yang *et al.* 2015*b*).

The non-adakitic granitoids have relatively low MgO (< 2 wt%) and Mg no. (< 41) (Table 2), different from those formed by assimilation and fractional crystallization of mantle-derived magmas with elevated MgO and Mg no. (Grove *et al.* 2003; Yang *et al.* 2019*c*). The non-adakitic granitoids show no differential trends of fractional crystallization of mantle-derived magma (Cai *et al.* 2015), and their Th contents (2.4–3.69 ppm) are also inconsistent with assimilation and fractional crystallization of mantle-derived magmas (Rapp & Waston, 1995; Cai *et al.* 2015). In addition, the non-adakitic granitoids contain no mafic enclaves or show no disequilibrium textures, implying that they could not result from the mixing of crustal and mantle-derived magmas. However, their low Cr (< 10 ppm), Ni (< 8 ppm) and Mg no. (< 41), and high K_2O (> 3 wt%), Th (> 2.4 ppm) and Rb (> 20 ppm), Rb/Sr (> 0.1) and La/Ce (> 0.45) are similar to those of I-type granitoids derived from middle or lower arc crust (Rapp & Watson, 1995; Skjerlie & Patiño Douce, 2002). The non-adakitic granitoids are therefore similar to the I-type granitoids derived from partial melts of thickened lower crust (Cai *et al.* 2015) or amphibolite and eclogite at pressures of 1.0–4.0 GPa (Fig. 9a; Rapp *et al.* 1991; Rapp, 1995; Cai *et al.* 2015).

In a subduction setting, the slab-derived fluids could induce partial melting of the mantle-wedge, and the ascending melts could change the mechanical and thermal states at the base of the arc crust and provide abundant heat for partial melting of middle–lower arc crust (Petford & Gallagher, 2001; Smith *et al.* 2003; Ren *et al.* 2014). Chemically, the Saleinuohai granite with higher SiO_2 contents resembles the rhyolites with SiO_2 contents of 69–79 wt% in the Izu–Bonin arc, which were produced by dehydration melting of middle crust (Tamura & Tatsumi, 2002). The Tangbale quartz-monzonite with lower SiO_2 and higher Cr and Ni contents is more like the melts of lower arc crust in Kermadec (65–73 wt%;

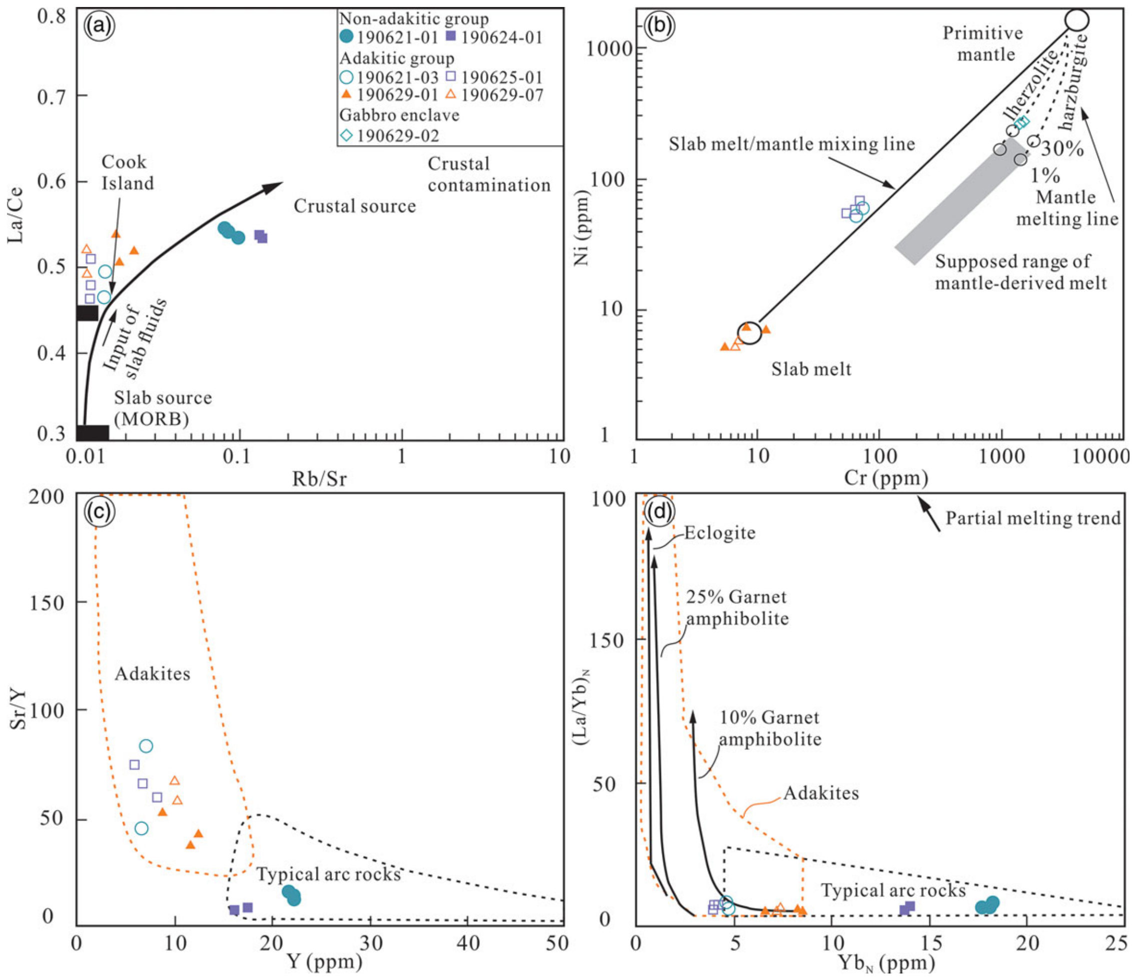

Fig. 10. (Colour online) (a) Rb/Sr versus La/Ce diagram showing that the adakitic and non-adakitic rocks are mainly slab- and crust-derived, respectively (after Hou *et al.* 2004). Data for the Cook Island adakite are from Stern & Kilian (1996). (b) Cr versus Ni diagram showing that mantle components were involved in the adakitic rocks (after Tsuchiya *et al.* 2005). (c) Y versus Sr/Y (after Defant & Drummond, 1990). (d) Yb_N versus $(La/Yb)_N$ (after Martin, 1999). The partial melting trends are based on diagrams from Zhou *et al.* (2006) showing that the igneous tectonic blocks are adakites or typical arc rocks.

Smith *et al.* 2003) and South Sandwich (63–73 wt%; Leat *et al.* 2003). Experimentally, the melts have increasing Al_2O_3 and Sr concentrations and Sr/Y ratios and decreasing Y and HREE concentrations as pressure increases (Petford & Atherton, 1996). The Tangbale quartz-monzonite has relatively enriched LREE ($(La/Yb)_N = 5.81–7.05$) and flat HREE with Y/Yb = 7.6–7.8, suggesting no garnet in source (Fig. 10d; Ge *et al.* 2002; Zhu *et al.* 2009). The melts for the Tangbale quartz-monzonite were therefore derived from an amphibole-bearing protolith (Martin *et al.* 2005). By contrast, the Saleinuohai granite has lower Al_2O_3 (12.36–12.44 wt%), Sr (150–158 ppm), Sr/Y (9–11) and Y/Yb (5.8–6.7) than the Tangbale quartz-monzonite, suggesting that the source for the Saleinuohai granite was at a shallower depth.

The non-adakitic granitoids were therefore likely derived from partial melts of the middle–lower crust of an intra-oceanic arc, which was modified by subduction fluids (Leat *et al.* 2000; Nebel *et al.* 2007).

6.a.3. Gabbro enclave

The Tierekehuola gabbro is low K-tholeiitic (Fig. 7c), and has low TiO_2 (*c.* 0.5 wt%) and high Fe_2O_3 (*c.* 11 wt%) and MgO (*c.* 15 wt%), with Mg no. = 72–73; it could therefore not be formed by partial melting of lower crust (Fig. 9a; Rudnick & Gao, 2003; Feng *et al.* 2016). Its high Co (45.4–48.6 ppm), Ni (231–288 ppm), Cr (1120–1360 ppm) and V (236–246 ppm) concentrations are typical of mantle-derived magmas (Figs 9a, 10b) and its enriched LILEs and strongly depleted Nb, Ta, Zr and Hf (Fig. 8c, d) can be attributed to significant effects of slab-derived fluids (Th < 1.1 ppm, Nebel *et al.* 2007) on its source in the mantle wedge (Fig. 9c, d; Eiler *et al.* 2000; Grove *et al.* 2003; Yang *et al.* 2012*a*; Liu *et al.* 2020).

6.b. Tectonic implications

The adakitic and non-adakitic group rocks and gabbro enclave were all formed in an intra-oceanic arc setting (Figs 7d, 9b–d), as suggested by previous studies (Ren *et al.* 2014; Zheng *et al.* 2019; Liu *et al.* 2020).

6.b.1. Ediacaran initial subduction

The SSZ-type ophiolites are predominant in the Barleik–Mayile–Tangbale accretionary complexes (Yang *et al.* 2012*a*; Ren *et al.* 2014; Weng *et al.* 2016; Liu *et al.* 2020), and the oldest SSZ-type gabbro occurs within the Mayile ophiolitic mélange and was formed at 572 Ma (Yang *et al.* 2012*a*), coeval with the oldest arc diorite in the Tangbale accretionary complex (Zheng *et al.*

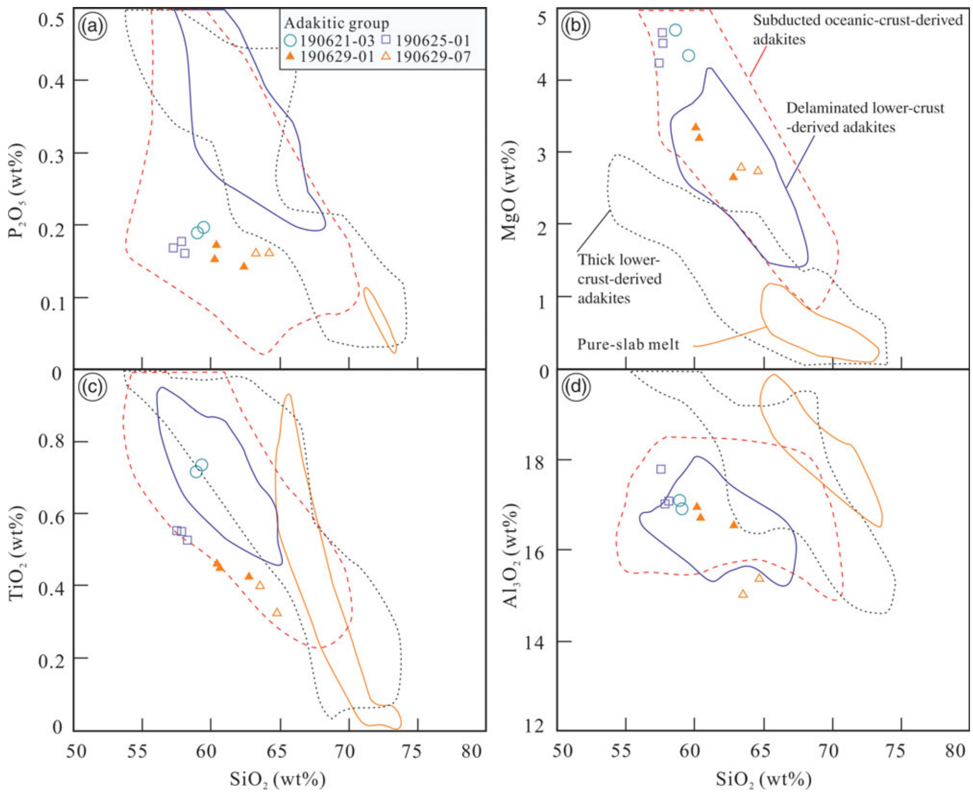

Fig. 11. (Colour online) SiO_2 versus (a) P_2O_5, (b) MgO, (c) TiO_2 and (d) Al_2O_3 diagrams showing that the adakitic rocks are consistent with subducted oceanic-crust-derived adakites. The fields of subducted oceanic-crust-derived, delaminated lower-crust-derived and thick lower-crust-derived adakites and pure slab melt are after Wang *et al.* (2006).

2019). This probably suggests that the subduction of the Junggar Ocean was initiated not later than 572 Ma (Zheng *et al.* 2019; Liu *et al.* 2020).

Both of the Tangbale adakitic monzonite and non-adakitic quartz-monzonite show arc affinities, but the Tangbale monzonite is calc-alkaline and was formed during the Ediacaran Period, followed by the high-K calc-alkaline quartz-monzonite at 549 Ma (this study) and quartz-diorite at *c.* 533 Ma (Fig. 7c; Zheng *et al.* 2019). If the subduction of Junggar Ocean was initiated at 572 Ma (Zheng *et al.* 2019; Liu *et al.* 2020), the transition from low-K tholeiitic series to high-K calc-alkaline series of arc magmatism characterizes the increasing arc maturity (Ishizuka *et al.* 2011; Ren *et al.* 2014).

6.b.2. Cambrian slab rollback

The Ediacaran–Cambrian igneous rocks show a N-wards younger trend, with the oldest Tangbale calc-alkaline monzonite at > 549 Ma, the youngest Tierekehuola low-K tholeiitic granodiorite at 530 Ma and the youngest Tierekehuola calc-alkaline diorite at 520 Ma. For the Cambrian arc magmatism, the Tierekehuola low-K tholeiitic granodiorite was formed at 530 Ma, earlier than the Saleinuohai calc-alkaline granite and monzonite at 529–524 Ma. This is the same as the across-arc compositional trend of tholeiitic to calc-alkaline with increasing distance from the trench (Tatsumi & Eggins, 1995; Ren *et al.* 2014), suggesting a S-directed subduction of oceanic lithosphere and a N-wards migration of arc magmatism. Such a temporal and spatial distribution of arc magmatism probably resulted from a N-wards rollback of the subducting slab during the Cambrian Period. Accordingly, late Cambrian adakitic and non-adakitic plutonic blocks in the accretionary complexes of southern West Junggar (Xu *et al.* 2012; Ren *et al.* 2014; Zheng *et al.* 2019) and plagiogranite block in the North Balkhash mélange, Central Kazakhstan (Degtyarev *et al.* 2021) may also have been formed during the slab rollback.

In summary, the S-directed subduction of the Junggar Ocean was initiated during the Ediacaran Period and resulted in the oldest SSZ-type ophiolite of 572 Ma (Yang *et al.* 2012*a*; Liu *et al.* 2020). The partial melting of subducted slab generated the adakitic rocks, followed by the partial melting of lower arc crust to form the non-adakitic rocks in an immature intra-oceanic arc (Fig. 12a). Possibly, the N-wards slab rollback and retreat of subduction zone occurred at *c.* 540 Ma, accompanied by the formation of younger SSZ-type ophiolites of 531 Ma (Jian *et al.* 2005; Weng *et al.* 2016). The Cambrian slab rollback induced the asthenospheric upwelling, which resulted in partial melting of the fluid-metamotized mantle-wedge to form the gabbro enclave as part of another immature arc. Afterwards, the partial melting of the oceanic slab and middle arc crust generated adakitic and non-adakitic magmas, respectively, and the gabbro enclave was wrapped by the adakitic pluton at 520–530 Ma (Fig. 12b).

7. Conclusions

(1) New LA-ICP-MS zircon U–Pb dating confirms the presence of Ediacaran–Cambrian igneous rocks in southern West Junggar region, and they can be divided into adakitic and non-adakitic groups.
(2) The adakitic rocks were generated by partial melting of subducted oceanic crust, but the melts were modified by mantle wedge and slab-derived fluids. The non-adakitic rocks were

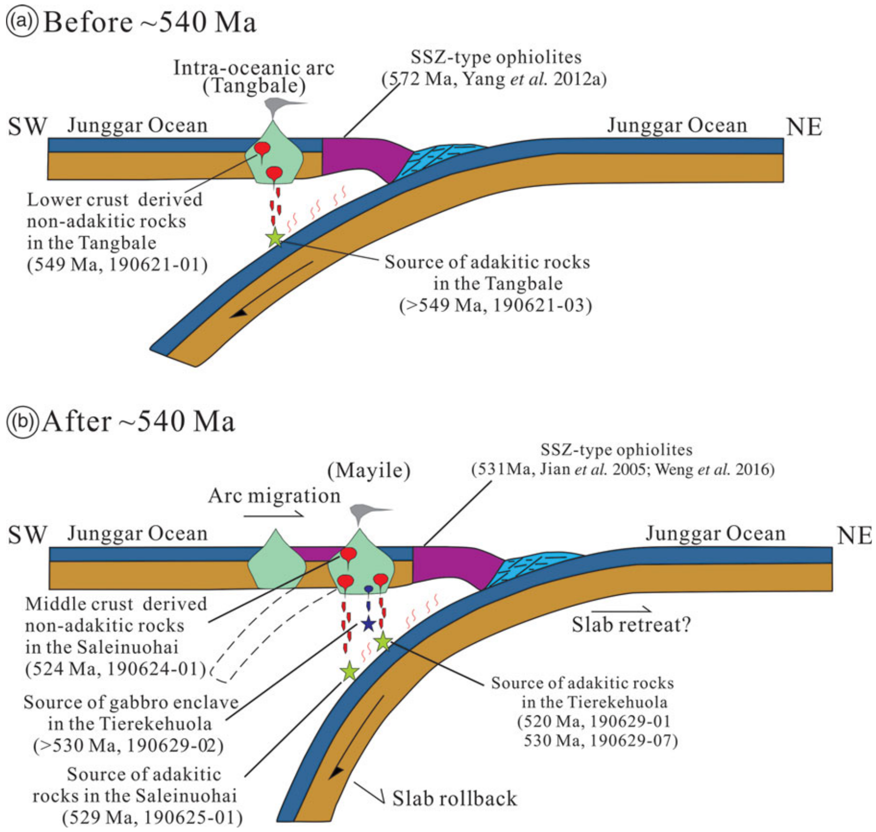

Fig. 12. (Colour online) A model for tectonic evolution of the Junggar Ocean during the Ediacaran–Cambrian periods.

derived from partial melts of the middle–lower crust of an intra-oceanic arc, which was modified by subduction fluids. In addition, the gabbro was formed as part of another immature arc by partial melting of the fluid-metasomatized mantle-wedge and then wrapped by adakitic granodiorite at 530–520 Ma.

(3) A N-wards younger trend of intra-oceanic arc magmatism could be generated by a process of Ediacaran initial subduction and Cambrian slab rollback of the Junggar Ocean.

Acknowledgements. We are grateful to Hao Sun, Bo Liu, Pan Zhao and Chong-Jin Pang for their help during fieldwork and article preparation. We thank the editor Dr Kathryn Goodenough and two anonymous reviewers for their constructive comments, which greatly improved the manuscript. We also thank copy-editor Elaine Rowan for corrections to language. This study was supported by the National Natural Science Foundation of China (grant no. 41972234), National Key R&D Program of China (grant no. 2017YFC0601203) and Opening Foundation of Hebei Key Laboratory of Strategic Critical Mineral Resources, Hebei GEO University (grant no. HGU-RGMKF211).

Supplementary material. To view supplementary material for this article, please visit https://doi.org/10.1017/S0016756821000376

References

Agard P, Yamato P, Soret M, Prigent C, Guillot S, Plunder A, Dubacg B, Chauvet A and Monie P (2016) Plate interface rheological switches during subduction infancy: Control on slab penetration and metamorphic sole formation. *Earth and Planetary Science Letters* **451**, 208–20.

Alexeiev DV, Ryazantsev AV, Kröner A, Tretyakov AA, Xia X and Liu DY (2011) Geochemical data and zircon ages for rocks in a high-pressure belt of Chu-Yili Mountains, southern Kazakhstan: implications for the earliest stages of accretion in Kazakhstan and the Tianshan. *Journal of Asian Earth Sciences* **42**, 805–20.

Anderson T (2002) Correction of common lead in U-Pb analyses that do not report ^{204}Pb. *Chemical Geology* **192**, 59–79.

Ashraf T, Tanya F, Nafiseh S and Kyle V (2019) Petrogenesis of adakites from the Sheyda volcano, NW Iran. *Journal of African Earth Sciences* **150**, 194–204.

Bellot N, Boyet M, Doucelance R, Bonnand P, Savov IP, Plank T and Elliott T (2018) Origin of negative cerium anomalies in subduction-related volcanic samples: constraints from Ce and Nd isotopes. *Chemical Geology* **500**, 46–63.

Buckman S and Aitchison JC (2001) Middle Ordovician (Llandeilan) radiolarians from West Junggar, Xinjiang, China. *Micropaleotology* **47**, 359–67.

Bureau of Geology and Mineral Resources of Xinjiang Uygur Autonomous Region (BGMRXUAR) (1993) *Regional Geology of Xinjiang Uygur Autonomous Region*. Beijing: Geological Publishing House (in Chinese with English abstract).

Cai YF, Wang YJ, Cawood PA, Zhang YZ and Zhang AM (2015) Neoproterozoic crustal growth of the Southern Yangtze Block: geochemical and zircon U-Pb geochronological and Lu-Hf isotopic evidence of Neoproterozoic diorite from the Ailaoshan zone. *Precambrian Research* **266**, 137–49.

Chen JF, Han BF, Ji JQ, Zhang L, Xu Z, He GQ and Wang T (2010) Zircon U-Pb ages and tectonic implications of Paleozoic plutons in northern West Junggar, North Xinjiang, China. *Lithos* **115**, 137–52.

Chen JF, Han BF, Zhang L, Xu Z, Liu JL, Qu WJ, Li C, Yang JH and Yang YH (2015) Middle Paleozoic initial amalgamation and crustal growth in the West Junggar (NW China): constraints from geochronology, geochemistry and Sr-Nd-Hf-Os isotopes of calc-alkaline and alkaline intrusions in the Xiemisitai-Saier Mountains. *Journal of Asian Earth Sciences* **113**, 90–109.

Chiaradia M (2009) Adakite-like magmas from fractional crystallization and melting assimilation of mafic lower crust (Eocene Macuchi arc, Western Cordillera, Ecuador). *Chemical Geology* **265**, 468–87.

Choulet F, Cluzel D, Faure M, Lin W, Wang B, Chen Y, Wu FY and Ji WB (2012) New constraints on the pre-Permian continental crust growth of Central Asia (West Junggar, China) by U-Pb and Hf isotopic data from detrital zircon. *Terra Nova* **24**, 189–98.

Choulet F, Faure M, Cluzel D, Chen Y, Lin W, Wang B and Xu B (2016) Toward a unified model of Altaids geodynamics: insight from the Palaeozoic polycyclic evolution of West Junggar (NW China). *Science China Earth Sciences* **59**, 25–57.

Defant M and Drummond MS (1990) Derivation of some modern arc magmas by melting of young subducted lithosphere. *Nature* **347**, 662–65.

Defant MJ and Kapezhinskas P (2001) Evidence suggests slab melting in arc magmas. *EOS, Transactions of the American Geophysical Union* **82**, 65–69.

Degtyarev KE, Luchitskaya MV, Tretyakov AA, Pilitsyna AV and Yakubchuk AS (2021) Early Paleozoic suprasubduction complexes of the North Balkhash ophiolite zone (Central Kazakhstan): geochronology, geochemistry and implications for tectonic evolution of the Junggar-Balkhash Ocean. *Lithos* **380–381**, 1–21.

Du HY and Chen JF (2017) The determination of Hobokesar ancient oceanic basin in west Junggar: evidence from zircon U-Pb age geochemistry of the Hobokesar ophiolitic mélange. *Acta Geologica Sinica* **91**, 2638–50 (in Chinese with English abstract).

Eiler JM, Crawford A, Elliott T, Farley KA, Valley JW and Stolper EM (2000) Oxygen isotope geochemistry of oceanic arc lavas. *Journal of Petrology* **41**, 229–56.

Elburg MA, van Bergen M, Hoogewerff J, Foden J, Vroon P, Zulkarnain I and Nasution A (2002) Geochemical trends across an arc-continent collision zone: magma sources and slab wedge transfer processes below the Pantar Strait volcanoes, Indonesia. *Geochimica et Cosmochimica Acta* **66**, 2771–89.

Ernst WG (2010) Subduction zone metamorphism, calc-alkaline magmatism, and convergent margin crustal evolution. *Gondwana Research* **18**, 8–16.

Feng ZQ, Liu YJ, Liu BQ, Wen QB, Li WM and Liu Q (2016) Timing and nature of the Xinlin-Xigutu Ocean: constraints from ophiolitic gabbros in the northern Great Xing'an Range, eastern Central Asian Orgenic Belt. *International Journal of Earth Sciences* **105**, 491–505.

Ge XY, Li XH, Chen ZG and Li WP (2002) Geochemistry and petrogenesis of Jurassic high Sr/Y low granitoids in eastern China: constrains on crustal thickness. *China Science Bulletin* **47**, 962–80.

Gordienko IV, Bulgatov AN, Lastochkin NI and Sitnikova VS (2009) Composition and U-Pb isotopic age determinations (SHRIMP II) of the ophiolitic assemblage from the Shaman paleospreading zone and the conditions of its formation (North Transbaikalia). *Doklady Earth Sciences* **429**, 1420–25.

Grove TL, Elkins-Tanton LT, Parman SW, Chatterjee N, Muntener O and Gaetani GA (2003) Fractional crystallization and mantle-melting control on calc-alkaline differentiation trends. *Contribution to Mineralogy and Petrology* **145**, 515–33.

Guilmette C, Smit MA and van Hinsbergen DJJ (2018) Forced subduction initiation recorded in the sole and crust of the Semail Ophiolite of Oman. *Nature Geoscience* **11**, 688–95.

Han BF, He GQ and Guo ZJ (2010) Timing of major suture zones in North Xinjiang, China: constraints from stitching plutons. *Acta Petrologica Sinica* **26**, 2233–46 (in Chinese with English abstract).

Han BF, Ji JQ, Song B, Chen LH and Zhang L (2006) Late Paleozoic vertical growth of continental crust around the Junggar Basin, Xinjiang, China (Part I): timing of post-collisional plutonism. *Acta Petrologica Sinica* **22**, 1077–86 (in Chinese with English abstract).

Hawkesworth C, Turner S, Peate D, Mcdermott F and Calsteren PV (1997) Elemental U and Th variations in island arc rocks: implications for U-series isotopes. *Chemical Geology* **139**, 207–21.

Hou ZQ, Gao YF, Qu XM, Rui ZY and Mo XX (2004) Origin of adakitic intrusives generated during mid-Miocene east-west extension in southern Tibet. *Earth and Planetary Science Letters* **220**, 139–55.

Ishizuka O, Tani K, Regan MK, Kanayama K, Umino S, Harigane Y, Sakamoto I, Miyajima Y and Yuasa M (2011) The timescales of subduction initiation and subsequent evolution of an oceanic island arc. *Earth and Planetary Science Letters* **306**, 229–40.

Jian P, Liu DY, Shi YR and Zhang FQ (2005) SHRIMP dating of SSZ ophiolites from northern Xinjiang province, China: implications for generation of oceanic crust in the Central Asian Orogenic belt. In *Structural and Tectonic Correlation across the Central Asia Orogenic Collage: North-Eastern Segment* (ed. Sklyarov EV). Guidebook and Abstract Volume of the Siberian Workshop ICCP-480, ICE SBRAS. Irkutsk: Institute of the Earth's crust of the Siberian Branch of Russian Academy of Sciences, pp. 246.

Khain EV, Bibikova EV, Kröner A, Zhuravlev DZ, Sklyarov EV, Fedotova AA and Kravchenko-Berezhnoy IR (2002) The most ancient ophiolite of the Central Asian fold belt: U-Pb and Pb-Pb zircon ages for the Dunzhugur Complex, Eastern Sayan, Siberia, and geodynamic implications. *Earth and Planet Science Letters* **199**, 311–25.

Konopelko D and Klemd R (2016) Deciphering protoliths of the (U) HP rocks in the Makbal metamorphic complex, Kyrgyzstan: geochemistry and SHRIMP zircon geochronology. *European Journal of Mineralogy* **28**, 1233–53.

Konopelko D, Kullerud K, Apayarov F, Sakiev K, Baruleva O, Ravna E and Lepekhina E (2012) SHRIMP zircon chronology of HP-UHP rocks of the Makbal metamorphic complex in the Northern Tien Shan, Kyrgyzstan. *Gondwana Research* **22**, 300–9.

Konopelko D, Seltmann R, Dolgopolova A, Safonova I, Glorie S, De Grave J and Sun M (2021) Adakite-like granitoids of Songkultau: a relic of juvenile Cambrian arc in Kyrgyz Tien Shan. *Geoscience Frontiers* **12**, 147–60.

Kröner A, Fedotova AA, Khain EV, Razumovskiy AA, Orlova AV, Anosova MO, Perelyaev VI, Nekrasov GE and Liu DY (2015) Neoproterozoic ophiolite and related high-grade rocks of the Baikal–Muya belt, Siberia: Geochronology and geodynamic implications. *Journal of Asian Earth Sciences* **111**, 138–60.

Kröner A, Windley BF, Badarch G, Tomurtogoo O, Hegner E, Jahn B.M, Gruschka S, Khain EV, Demoux A and Wingate MTD (2007) Accretionary growth and crust formation in the Central Asian Orogenic Belt and comparison with the Arabian-Nubian shield. In *4-D Framework of Continental Crust* (eds RD Hatcher, MP Carlson, JH McBride, JR Martínez Catalán), pp. 181–209. Boulder: Geological Society of America, Memoir no. **200**.

Kwon ST, Tilton GR, Coleman RG and Feng Y (1989) Isotopic studies bearing on the tectonics of the west Junggar region, Xinjiang, China. *Tectonics* **8**, 719–27.

Leat PT, Livermore RA, Millar IL and Pearce JA (2000) Magma supply in back arc spreading centre segment E2, east Scotia Ridge. *Journal of Petrology* **41**, 845–66.

Leat PT, Smellie JL, Millar IL and Larter RD (2003) Magmatism in the South Sandwich arc. In *Intra-Oceanic Subduction Systems: Tectonic and Magmatic Processes* (eds RD Larter and PT Leat), pp. 285–314. Geological Society of London, Special Publication no. **219**.

Li D, He DF, Qi XF and Zhang NN (2015) How was the Carboniferous Balkhash-West Junggar remnant ocean filled and closed? Insights from the Well Tacan-1 strata in the Tacheng Basin, NW China. *Gondwana Research* **27**, 342–62.

Liu B, Han BF, Ren R, Chen JF, Wang ZZ and Zheng B (2017) Petrogenesis and tectonic implications of the Early Carboniferous to the Late Permian Barleik plutons in the West Junggar (NW China). *Lithos* **272-273**, 232–48.

Liu B, Han BF, Xu Z, Ren R and Chen JF (2020) The Ediacaran to Early Palaeozoic evolution of the Junggar-Balkhash Ocean: a synthesis of the ophiolitic mélanges in the southern West Junggar terrane, NW China. *Geological Journal* **55**, 1689–707.

Liu B, Han BF, Xu Z, Ren R, Zhang JR, Zhou J, Su L and Li QL (2016) The Cambrian initiation of intra-oceanic subduction in the southern Paleo-Asian Ocean: further evidence from the Barleik subduction-related metamorphic complex in the West Junggar region, NW China. *Journal of Asian Earth Sciences* **123**, 1–21.

Liu JH, Xie CM, Li C, Fan JJ, Wang M, Wang W, Yu YP, Dong YC and Hao YJ (2019) Origins and tectonic implications of Late Cretaceous adakite and primitive high-Mg andesite in the Songdo area, southern Lhasa subterrane, Tibet. *Gondwana Research* **76**, 185–203.

Liu JH, Xie CM, Li C, Wang M, Wu H, Li XK, Liu YM and Zhang TY (2018) Early Carboniferous adakite-like and I-type granites in central Qiangtang, northern Tibet: implications for intra-oceanic subduction and back-arc basin formation within the Paleo-Tethys Ocean. *Lithos* **296-299**, 265–80.

Liu YS, Gao S, Hu ZC, Gao CG, Zong KQ and Wang DB (2010) Continental and oceanic crust recycling-induced melt-peridotite interactions in the Trans-North China Orogen: U-Pb dating, Hf isotopes and trace elements in zircons from mantle xenoliths. *Journal of Petrology* **51**, 537–71.

Ludwig KR (2012) *User's Manual for Isoplot 3.75: A Geochronological Toolkit for Microsoft Excel*. Berkeley: Berkeley Geochronology Center, 75 p.

Ma L, Wang Q, Wyman DA, Li ZX, Jiang ZQ, Yang JH, Gou GN and Guo HF (2013) Late Cretaceous (100-89 Ma) magnesian charnockites with adakitic affinities in the Milin area, eastern Gangdese: partial melting of subducted oceanic crust and implications for crustal growth in southern Tibet. *Lithos* **175-176**, 315–32.

Maniar PD and Piccoli PM (1989) Tectonic discrimination of granitoids. *Geological Society of America Bulletin* **101**, 635–43.

Martin H (1999) Adakitic magmas: modern analogues of Archaean granitoids. *Lithos* **46**, 411–29.

Martin H, Smithies R, Rapp R, Moyen J and Champion D (2005) An overview of adakite, tonalite-trondhjemite-granodiorite (TTG), and sanukitoid: relationships and some implications for crustal evolution. *Lithos* **79**, 1–24.

Meyer M, Klemd R and Konopelko D (2013) High-pressure mafic oceanic rocks from the Makbal Complex, Tianshan Mountains (Kazakhstan and Kyrgyzstan): implications for the metamorphic evolution of a fossil subduction zone. *Lithos* **177**, 207–25.

Middlemost EAK (1994) Naming materials in the magma/igneous rock system. *Earth Science Review* **37**, 215–24.

Nebel O, Münker C, Nebel-Jacobsen YJ, Kleine T, Mezger K and Mortimer N (2007) Hf-Nd-Pb isotope evidence from Permian arc rocks for the long-term presence of the Indian Pacific mantle boundary in the SW Pacific. *Earth and Planetary Science Letters* **254**, 377–92.

Nekrasov GE, Rodionov NV, Berezhnaya NG, Sergeev SA, Ruzhentsev SV, Minina OR and Golionko BG (2007) U-Pb Age of zircons from plagiogranite veins in migmatized amphibolites of the Shaman Range (Ikat-Bagdarin zone, Vitim Highland, Transbaikal region). *Doklady Earth Sciences* **413**, 160–63.

Pearce JA (2008) Geochemical finger printing of oceanic basalts with applications to ophiolite classification and the search for Archean oceanic crust. *Lithos* **100**, 4–48.

Pearce JA, Harris NBW and Tindle AG (1984) Trace element discrimination diagrams for the tectonic interpretation of granitic rocks. *Journal of Petrology* **25**, 956–83.

Peccerillo A and Taylor SR (1976) Geochemistry of eocene calc-alkaline volcanic rocks from the Kastamonu area, Northern Turkey. *Contributions to Mineralogy and Petrology* **58**, 63–81.

Petford N and Atherton M (1996) Na-rich partial melt from newly underplated basa1tic crust, the Cordillera Blanca Batholith, Peru. *Journal of Petrology* **37**, 49l–52l.

Petford N and Gallagher K (2001) Partial melting of mafic (amphibolitic) lower crust by periodic influx of basaltic magma. *Earth and Planet Science Letters* **193**, 483–99.

Rapp RP (1995) Amphibole-out phase boundary in partially melted metabasalt, its control over liquid fraction and composition, and source permeability. *Journal of Geophysical Research, Solid Earth* **100**, 15601–10.

Rapp RP, Shimizu N, Norman MD and Applegate GS (1999) Reaction between slab-derived melts and peridotite in the mantle wedge: experimental constraints at 3.8 GPa. *Chemical Geology* **160**, 335–56.

Rapp RP and Watson EB (1995) Dehydration melting of metabasalt at 8-32 kbar: implications for continental growth and crust-mantle recycling. *Journal of Petrology* **36**, 891–931.

Rapp RP, Watson EB and Miller CF (1991) Partial melting of amphibolite/eclogite and the origin of Archean trondhjemites and tonalites. *Precambrian Research* **51**, 1–25.

Ren R, Han BF, Xu Z, Zhou YZ, Liu B, Zhang L, Chen JF, Su L, Li J, Li XH and Li QL (2014) When did the subduction first initiate in the southern Paleo-Asian Ocean: new constraints from a Cambrian intra-oceanic arc system in West Junggar, NW China. *Earth and Planetary Science Letters* **388**, 222–36.

Rudnick RL and Gao S (2003) Composition of the continental crust. In *Treatise on Geochemistry* (eds KK Turekian and HD Holland), pp. 1–64. Amsterdam: Elsevier Science.

Ryazantsev AV, Degtyarev KE, Kotov AB, Sal'nikova EB, Anisimova IV and Yakovleva SZ (2009) Ophiolite sections of the Dzhalair-Nayman zone, South Kazakhstan: their structure and age substantiation. *Doklady Earth Sciences* **427**, 902–6.

Sen C and Dunn T (1994) Dehydration melting of a basaltic composition amphibolite at 1.5 and 2.0 GPa: implications for the origin of adakites. *Contributions to Mineralogy and Petrology* **117**, 394–409.

She JZ, Deng HT, Liu G, Gao Q and Di XC (2016) Geochemical features and structural significance of Hongguleleng ophiolite in Western Junggar, Xinjiang. Xinjiang *Geology* **34**, 40–45 (in Chinese with English abstract).

Shen P, Shen YC, Li XH, Pan HD, Zhu HP, Meng L and Dai HW (2012) Northwestern Junggar Basin, Xiemisitai Mountains, China: a geochemical and geochronological approach. *Lithos* **140**, 103–18.

Sisson TW, Ratajeski K, Hankins WB and Glazner AF (2005) Voluminous granitic magmas from common basaltic sources. *Contributions to Mineralogy and Petrology* **148**, 635–61.

Skjerlie KP and Patiño Douce AE (2002) The fluid absent partial melting of a zoisite bearing quartz eclogite from 1.0 to 3.2 GPa: implications for melting in thickened continental crust and for subduction-zone processes. *Journal of Petrology* **43**, 291–314.

Sláma J, Kosler J, Condon DJ, Crowley JL, Gerdes A, Hanchar JM, Horstwood MSA, Morris GA, Nasdala L, Norberg N, Schaltegger U, Schoene B, Tubrettk MN and Whitehouse MJ (2008) Pleovice zircon: a new natural reference material for U-Pb and Hf isotopic microanalysis. *Chemical Geology* **249**, 1–35.

Smith IEM, Worthington TJ, Stewart RB, Price RC and Gamble JA (2003) Felsic volcanism in the Kermadec arc, SW Pacific: crustal recycling in an oceanic setting. In Intra-Oceanic Subduction Systems: Tectonic and Magmatic Processes (eds RD Larter and PT Leat), pp. 99–118. Geological Society of London, Special Publication no. **219**.

Smithies RH (2000) The Archaean tonalite-trondhjemite-granodiorite (TTG) series is not an analogue of Cenozoic adakite. *Earth and Planetary Science Letters* **182**, 115–25.

Stern CR and Kilian R (1996) Role of the subducted slab, mantle wedge, and continental crust in the generation of adakites from the Andean Austral Volcanic Zone. *Contributions to Mineralogy and Petrology* **123**, 263–81.

Stern RJ and Taras G (2018) Subduction initiation in nature and models: A review. *Tectonophysics* **746**, 173–98.

Streck MJ, Leeman WP and Chesley J (2007) High-Mg andesite from Mount Shasta: a product of magma mixing and contamination, not a primitive mantle melt. *Geology* **35**, 351–54.

Sun SS and McDonough WF (1989) Chemical and isotopic systematics of oceanic basalts: implications for mantle composition and processes. In *Magmatism in the Ocean Basins* (eds AD Saunders and MJ Norry), pp. 313–45. Geological Society of London, Special Publication no. **42**.

Tagiri M, Takiguchi S, Ishida C, Noguchi T, Kimura M, Bakirov A, Sakiev K, Takahashi M, Takasu A, Bakirov A, Togonbarva A and Suzuki A (2010) Intrusion of UHP metamorphic rocks into the upper crust of Kyrgyzian Tien-Shan: P-T path and metamorphic age of the Makbal Complex. *Journal of Mineralogical and Petrological Sciences* **105**, 233–50.

Tamura Y and Tatsumi Y (2002) Remelting of an andesitic crust as a possible origin for rhyolitic magma in oceanic arcs: an example from the Izu-Bonin arc. *Journal of Petrology* **43**, 1029–47.

Tatsumi Y and Eggins S (1995) *Subduction Zone Magmatism*. Cambridge: Blackwell Science.

Tsuchiya N, Suzuki S, Kimura J and Kagami H (2005) Evidence for slab melt/mantle reaction: petrogenesis of Early Cretaceous and Eocene high-Mg andesites from the Kitakami Mountains, Japan. *Lithos* **79**, 179–206.

Turkina OM, Nozhkin AD, Bibikova EV, Zhuravlev DZ and Travin AV (2004) The Arzybei Terrane: a fragment of the Mesoproterozoic island-arc crust in the southwestern framing of the Siberian craton. *Doklady Earth Sciences* **395**, 246–50.

Wang Q, Mcdermott F, Xu JF, Bellon H and Zhu YT (2005) Cenozoic K-rich adakitic volcanic rocks in the Hohxil area, northern Tibet: lower-crustal melting in an intracontinental setting. *Geology* **33**(6), 465–68.

Wang Q, Xu JF, Jian P, Bao ZW, Zhao ZH, Li CF, Xiong XL and Ma JL (2006) Petrogenesis of adakitic porphyries in and extensional tectonic setting,

Dexing, South China: implications for the Genesis of porphyry copper mineralization. *Journal of Petrology* **47**, 119–44.
Wang ZH, Sun S, Li JL, Hou QL, Qin KZ, Xiao WJ and Hao J (2003) Paleozoic tectonic evolution of the northern Xinjiang, China: Geochemical and geochronological constraints from the ophiolites. *Tectonics* **22**, 1–15.
Wen ZG, Zhao WP, Liu TF and Liu SB (2016) Formation age and geotectonic significance of Baerluke ophiolite in west Junggar, Xinjiang. *Geological Bulletin of China* **35**, 1401–10 (in Chinese with English abstract).
Weng K, Xu XY, Ma ZP, Chen JL, Sun JM, Zhang X (2016) The geochemistry and chronology characteristics and the geological significance of ultramafic rock in Mayile ophiolite, West Junggar, Xinjiang. *Acta Petrologica Sinica* **32**(5), 1420–36 (in Chinese with English abstract).
Windley BF, Alexeiev D, Xiao WJ, Kröner A and Badarch G (2007) Tectonic models for accretion of the Central Asian Orogenic Belt. *Journal of the Geological Society of London* **164**, 31–47.
Wood DA (1980) The application of a Th-Hf-Ta diagram to problems of tectonomagmatic classification and to establishing the nature of crustal contamination of basaltic lavas of the British Tertiary Volcanic Province. *Earth and Planetary Science Letters* **50**, 11–30.
Wu C, Hong T, Xu XW, Cao MJ, Li H, Zhang GL, You J, Ke Q and Dong LH (2018) Tectonic evolution of the Paleozoic Barluk continental arc, West Junggar, NW China. *Journal of Asian Earth Sciences* **160**, 48–66.
Wu H, Li C, Xu MJ and Li XK (2015) Early Cretaceous adakitic magmatism in the Dachagou area, northern Lhasa terrane, Tibet: implications for slab rollback and subsequent slab break-off of the lithosphere of the Bangong-Nujiang Ocean. *Journal of Asian Earth Sciences* **97**, 51–66.
Xiao WJ, Han CM, Yuan C, Sun M, Lin SF, Chen HL, Li ZL, Li JL and Shu S (2008) Middle Cambrian to Permian subduction-related accretionary orogenesis of northern Xinjiang, NW China: implications for the tectonic evolution of Central Asia. *Journal of Asian Earth Sciences* **32**, 102–17.
Xiao WJ, Windley B, Hao J and Zhai MG (2003) Accretion leading to collision and the Permian Solonker suture, Inner Mongolia, China: termination of the Central Asian Orogenic Belt. *Tectonics* **22**, 1069–89.
Xiao WJ, Windley BF, Sun S, Li JL, Huang BC, Han CM, Yuan C, Sun M and Chen HL (2015) A tale of amalgamation of three Permo-Triassic collage systems in Central Asia: oroclines, sutures, and terminal accretion. *Annual Review of Earth and Planetary Sciences* **43**, 477–507.
Xu QQ, Ji JQ, Zhao L, Gong JF, Zhou J and He GQ (2013a) Tectonic evolution and continental crust growth of Northern Xinjiang in northwestern China: Remnant ocean model. *Earth-Science Reviews* **126**, 178–205.
Xu X, He GQ, Li HQ, Ding TF, Liu XY and Mei SW (2006) Basic characteristics of the Karamay ophiolitic mélange, Xinjiang, and its zircon SHRIMP dating. *Geology of China* **33**, 470–75 (in Chinese with English abstract).
Xu Z, Han BF, Ren R, Zhou YZ and Su L (2013b) Palaeozoic multiphase magmatism at Barleik Mountain, southern West Junggar, Northwest China: implications for tectonic evolution of the West Junggar. *International Geology Review* **55**, 633–56.
Xu Z, Han BF, Ren R, Zhou YZ, Zhang L, Chen JF and Liu DY (2012) Ultramafic-mafic mélange, island arc and post-collisional intrusions in the Mayile Mountain, West Junggar, China: implications for Paleozoic intra-oceanic subduction-accretion process. *Lithos* **132**, 141–61.
Yang GX, Li YJ, Santosh M, Gu PY, Yang BK, Zhang B, Wang HB, Zhong X and Tong LL (2012a) A Neoproterozoic seamount in the Paleoasian Ocean: evidence from zircon U-Pb geochronology and geochemistry of the Mayile ophiolitic mélange in West Junggar, NW China. *Lithos* **140-141**, 53–65.
Yang GX, Li YJ, Santosh M, Yang BK, Yan J, Zhang B and Tong LL (2012b) Geochronology and geochemistry of basaltic rocks from the Sartuohai ophiolitic mélange, NW China: implications for a Devonian mantle plume within the Junggar Ocean. *Journal of Asian Earth Sciences* **59**, 141–55.
Yang GX, Li YJ, Tong LL, Wang ZP and Xu Q (2019a) Petrogenesis of pillow basalts in West Junggar, NW China: constraints from geochronology, geochemistry, and Sr-Nd-Pb isotopes. *Geological Journal* **54**, 1815–33.
Yang GX, Li YJ, Xiao WJ and Tong LL (2015a) OIB-type rocks within West Junggar ophiolitic mélanges: evidence for the accretion of seamounts. *Earth-Science Reviews* **150**, 477–96.
Yang GX, Li YJ, Yang BK, Wang HB, Zhang HW and Tong LL (2012c) Geochemistry of basalt from the Barleik ophiolitic mélange in West Junggar and its tectonic implications. *Acta Geology Sinica* **86**, 188–197 (in Chinese with English abstract).
Yang YQ, Zhao L, Zheng RG and Xu QQ (2019b) Evolution of the early Paleozoic Hongguleleng-Balkybey Ocean: Evidence from the Hebukesaier ophiolitic mélange in the northern West Junggar, NW China. *Lithos* **324-325**, 519–36.
Yang YQ, Zhao L, Xu QQ, Zheng RG, Liu JH and Zhang J (2019c) Early Paleozoic tectonic evolution of the northern West Junggar (NW China): constraints from Early Cambrian-Middle Silurian felsic plutons of the Chagantaolegai ophiolitic mélange. *Lithos* **350-351**, 105–25.
Yang ZM, Lu YJ, Hou ZQ and Chang ZS (2015b) High-Mg diorite from Qulong in Southern Tibet: implications for the genesis of adakite-like intrusions and associated Porphyry Cu deposits in collisional orogens. *Journal of Petrology* **56**, 227–54.
Yin J, Chen W, Xiao W, Yuan C, Windley BF, Yu S and Cai KD (2015) Late Silurian-early Devonian adakitic granodiorite, A-type and I-type granites in NW Junggar, NW China: partial melting of mafic lower crust and implications for slab roll-back. *Gondwana Research* **43**, 55–73.
Zhang C, Ma CQ, Holtz F, Koepke J, Wolff PE and Berndt J (2013) Mineralogical and geochemical constraints on contribution of magma mixing and fractional crystallization to high-Mg adakite-like diorites in eastern Dabie orogen, East China. *Lithos* **172-173**, 118–38.
Zhang C, Zhai M.G, Allen MB, Sanuders AD, Wang GR and Huang X (1993) Implications of Palaeozoic ophiolites from West Junggar, NW China, for the tectonics of Central Asia. *Journal of the Geological Society of London* **150**, 551–61.
Zhang JE, Xiao WJ, Luo J, Chen YC, Windley BF, Song DF, Han CM and Safonova I (2018a) Collision of the Tacheng block with the Mayile-Barleik-Tangbale accretionary complex in Western Junggar, NW China: Implication for Early-Middle Paleozoic architecture of the western Altaids. *Journal of Asian Earth Sciences* **159**, 259–78.
Zhang LF (1997) The $^{40}Ar/^{39}Ar$ metamorphic ages of Tangbale blueschists and their geological significance in West Junggar of Xinjiang. China *Science Bulletin* **42**, 1902–4.
Zhang LL, Zhu DC, Wang Q, Zhao ZD, Liu D and Xie JC (2019) Late Cretaceous volcanic rocks in the Sangri area, southern Lhasa Terrane, Tibet: evidence for oceanic ridge subduction. *Lithos* **326-327**, 144–57.
Zhang P, Wang GC, Polat A, Zhu CY, Shen TY, Chen Y, Chen C, Guo JS, Wu GL and Liu YT (2018b) Emplacement of the ophiolitic mélanges in the west Karamay area: implications for the Late Paleozoic tectonic evolution of West Junggar, northwestern China. *Tectonophysics*, **747-748**, 259–80.
Zhang Z, Zhao G, Santosh M, Wang J, Dong X and Shen K (2010) Late Cretaceous charnockite with adakitic affinities from the Gangdese batholith, southeastern Tibet: evidence for Neo-Tethyan mid-ocean ridge subduction? *Gondwana Research* **17**, 615–31.
Zhao WP, Jia ZK, Wen ZG and Li YJ (2012) The discovery of the blueschists from the Baerluke ophiolitic mélange belt in West Junggar, Xinjiang. Northwest *Geology* **45**, 136–38 (in Chinese with English abstract).
Zheng B, Han BF, Liu B and Wang ZZ (2019) Ediacaran to Paleozoic magmatism in West Junggar Orogenic Belt, NW China, and implications for evolution of Central Asian Orogenic Belt, *Lithos* **338-339**, 111–27.
Zhou MF, Yan DP, Wang CL, Qi L and Kennedy A (2006) Subduction-related origin of the 750Ma Xuelongbao adakitic complex (Sichuan province, China): implications for the tectonic setting of the giant neoproterozoic magmatic event in south China. *Earth and Planetary Science Letters* **248**, 286–300.
Zhu DC, Mo XX, Niu Y, Zhao ZD, Wang LQ, Liu YS and Wu FY (2009) Geochemical investigation of Early Cretaceous igneous rocks along an east-west traverse throughout the central Lhasa terrane, Tibet. *Chemical Geology* **268**, 298–312.
Zong RW, Wang ZH, Jiang T and Gong YM (2016) Late Devonian radiolarian-bearing siliceous rocks from the Karamay ophiolitic mélange in western Junggar: implications for the evolution of the Paleo-Asian Ocean. *Palaeogeography, Palaeoclimatology, Palaeoecology* **448**, 266–278.

https://doi.org/10.1017/S0016756821000376 Published online by Cambridge University Press